Cycle 24 and longer-term evolution of the solar photospheric and coronal magnetic field

Gordon Petrie, NSO

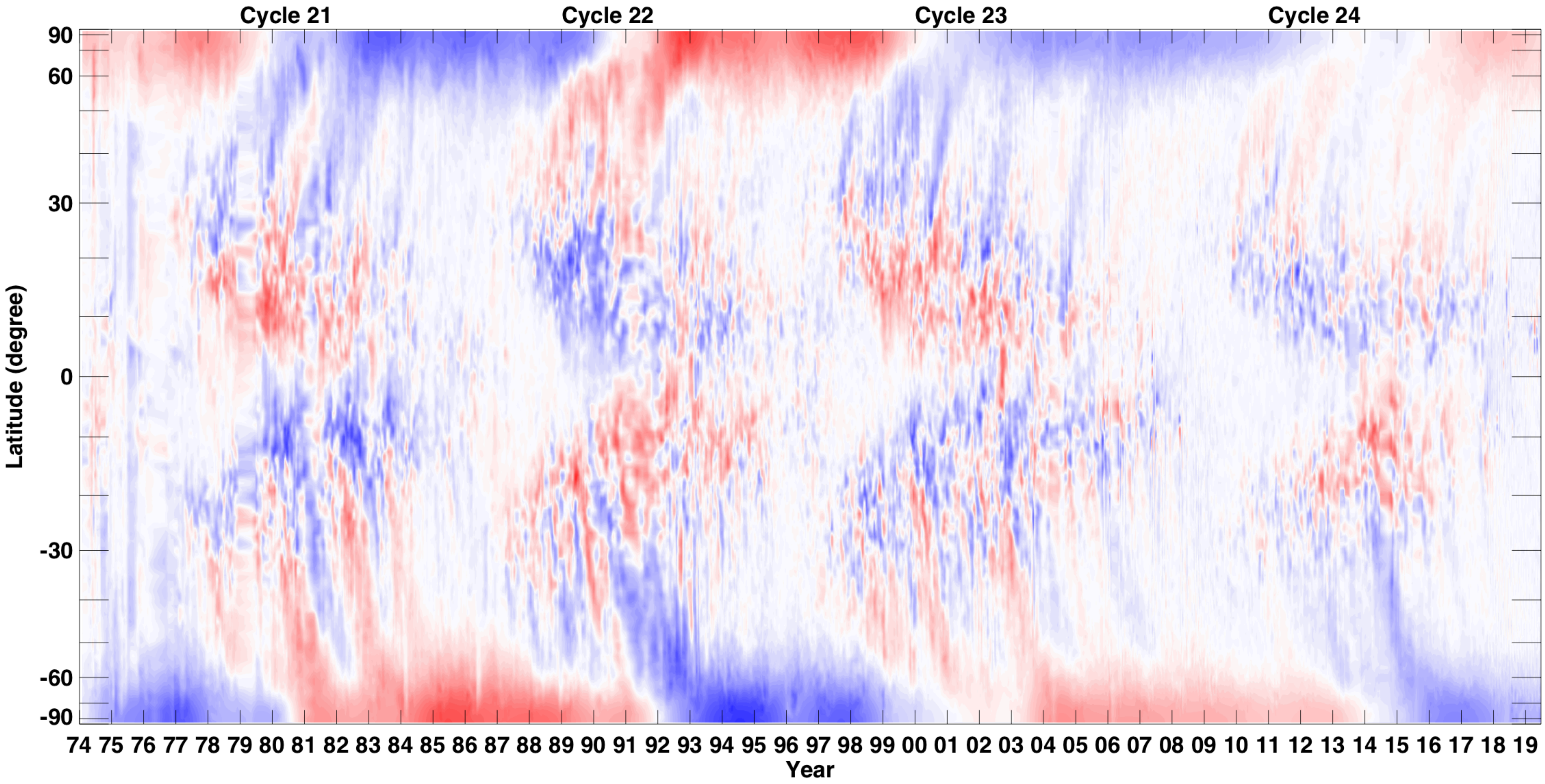

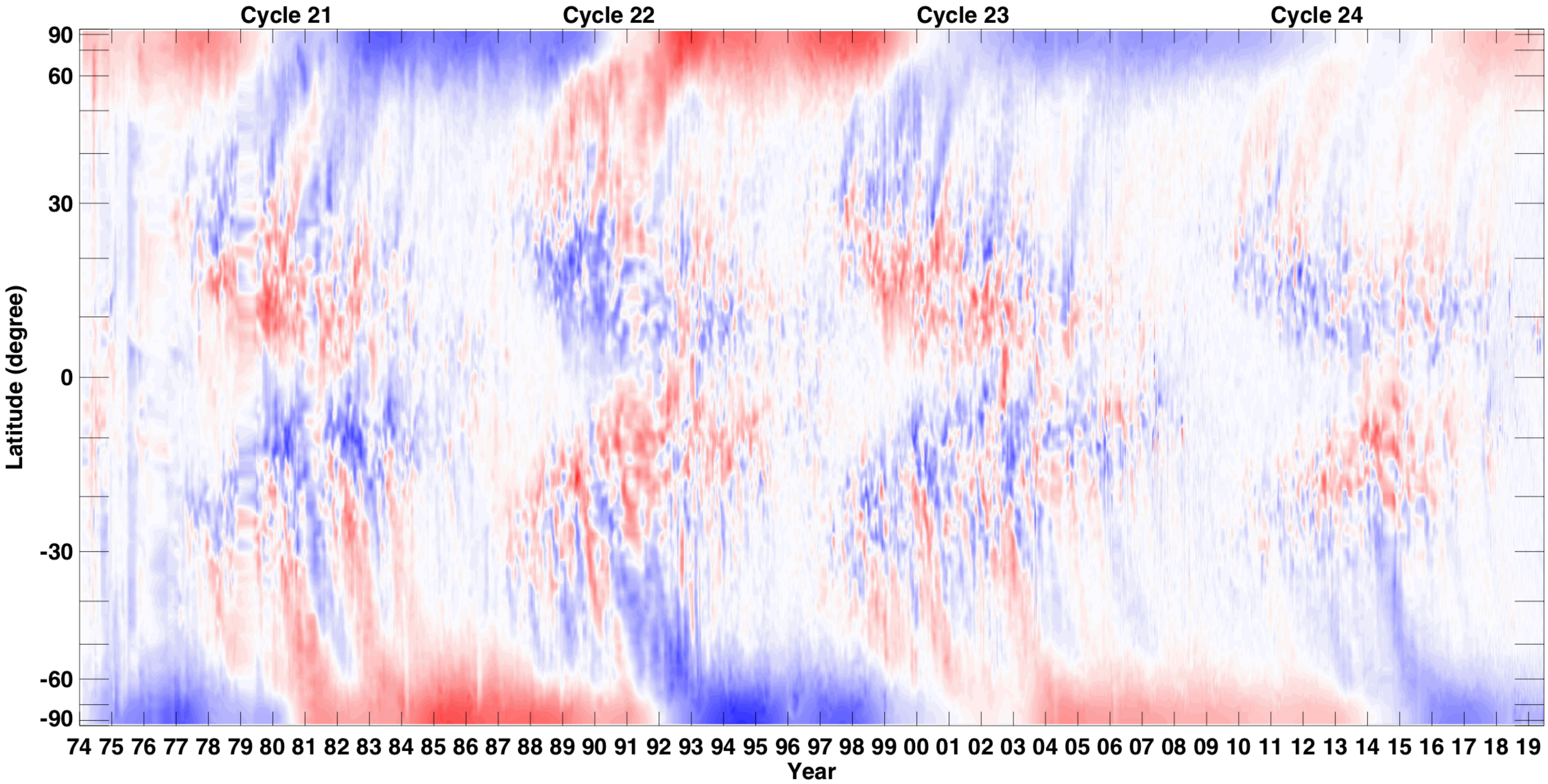

- Butterfly diagram of data from KPVT/512ch (74-92), KPVT/SPMG (92-03), SOLIS/VSM (03-17) & SDO/HMI (17-present). Red=positive, blue negative, saturates at ±15G.
- Decayed AR flux is transported from active latitudes to poles in unipolar surges. Polar fields respond to these surges.
- Polar reversals can be fast (cycle 21, 22) or slow (cycle 23 S, 24 N).
- Cycle 24 highlights: hemispheric activity asymmetry, asymmetric polar field changes, activity quietening down, polar fields close to maximum strength.

Total active-region magnetic flux

Solid: north hemisphere
dashed: south hemisphere

+ve flux
-ve flux

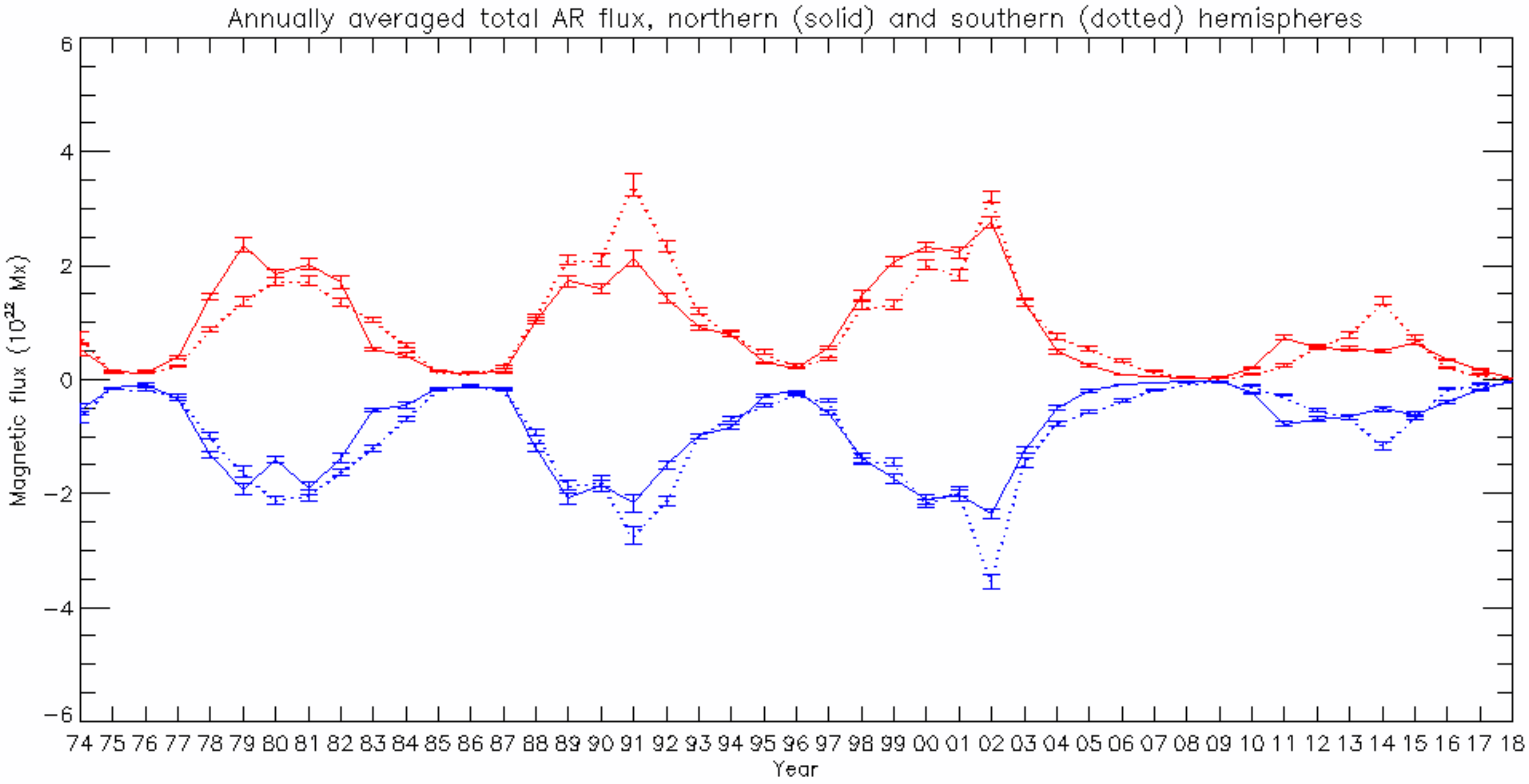

Cycle 24 activity level about 50% of Cycle 21-23 maxima according to total active-region fluxes, large hemispheric asymmetry.

Maximum AR field strength

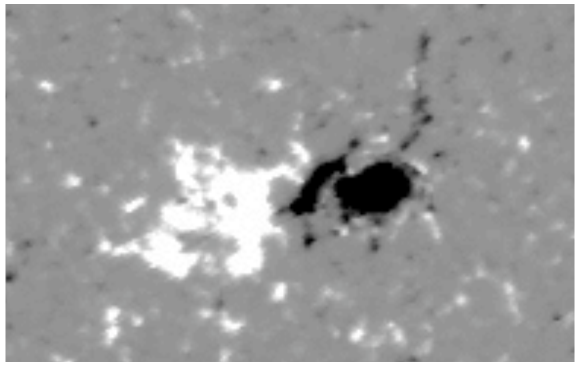

Solid: north hemisphere
dashed: south hemisphere

+ve flux
-ve flux

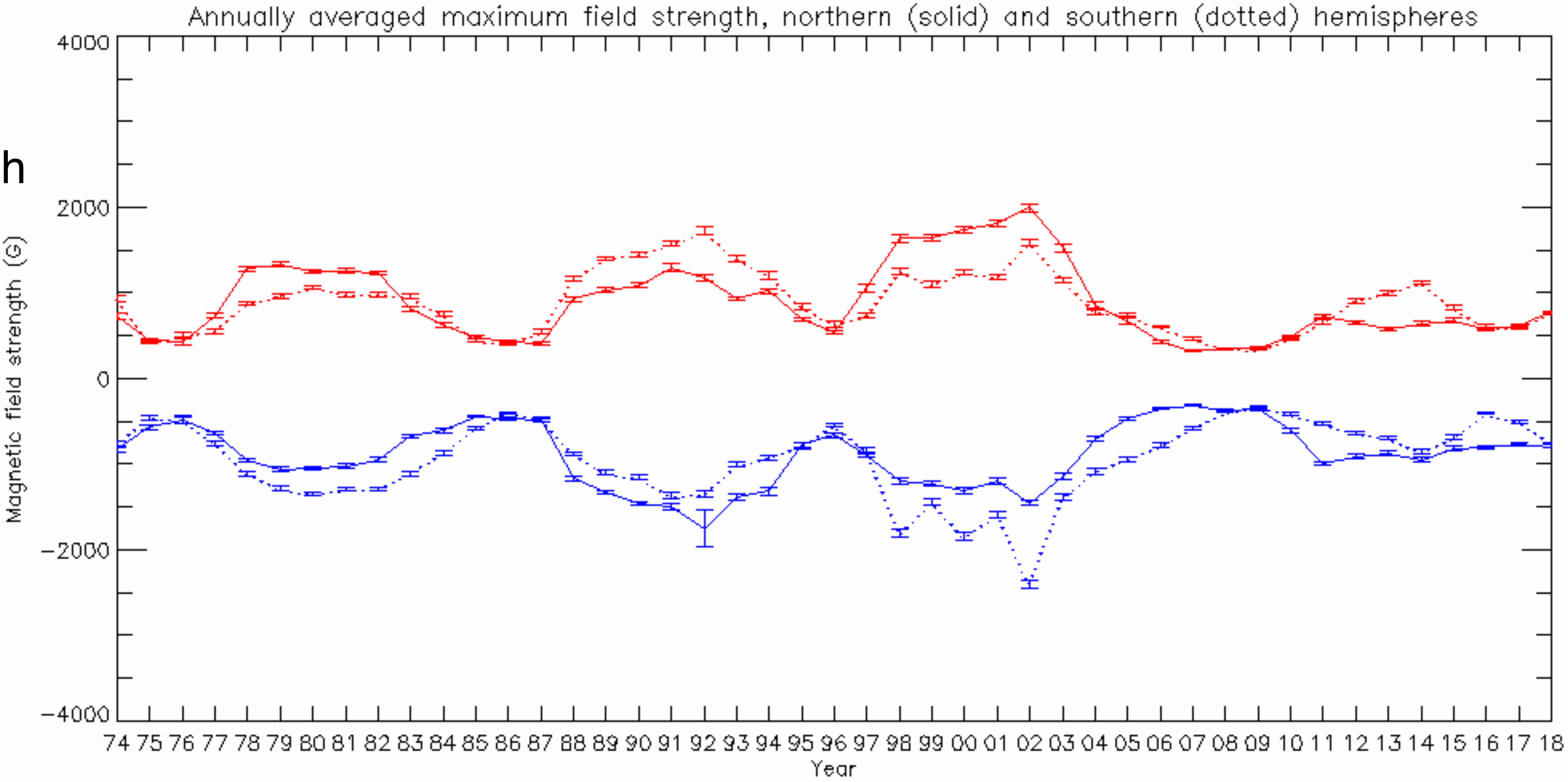

Cycle 24 activity level slightly weaker than Cycle 21-23 maxima. Bipole asymmetry is apparent during all cycles, although during decline of cycle 23 the hemispheric asymmetry briefly dominated.

MWO: Maximum AR field strength

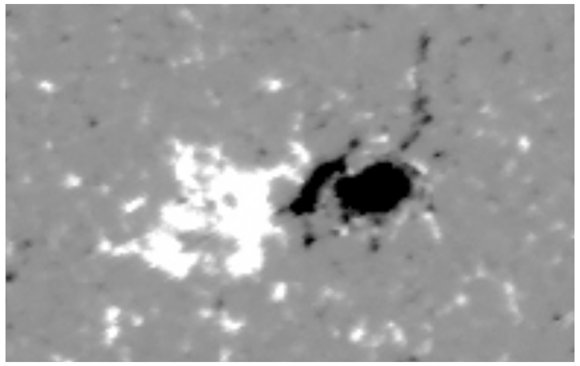

Solid: north hemisphere dashed: south hemisphere

+ve flux
-ve flux

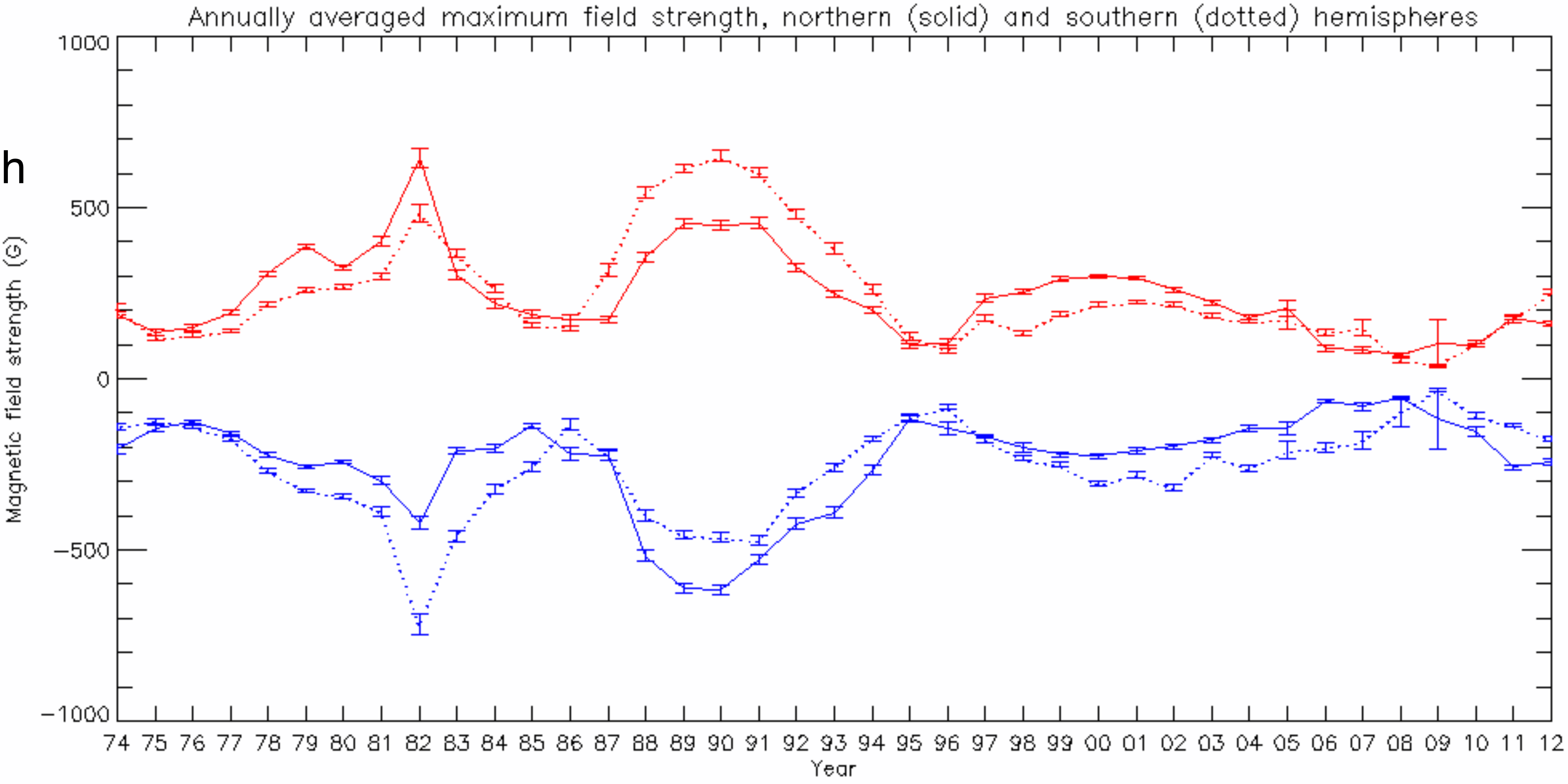

Bipole asymmetry is apparent, although between around 2004 and 2011 the hemispheric asymmetry dominates.

Annual fraction of images with fields stronger than 1 kG

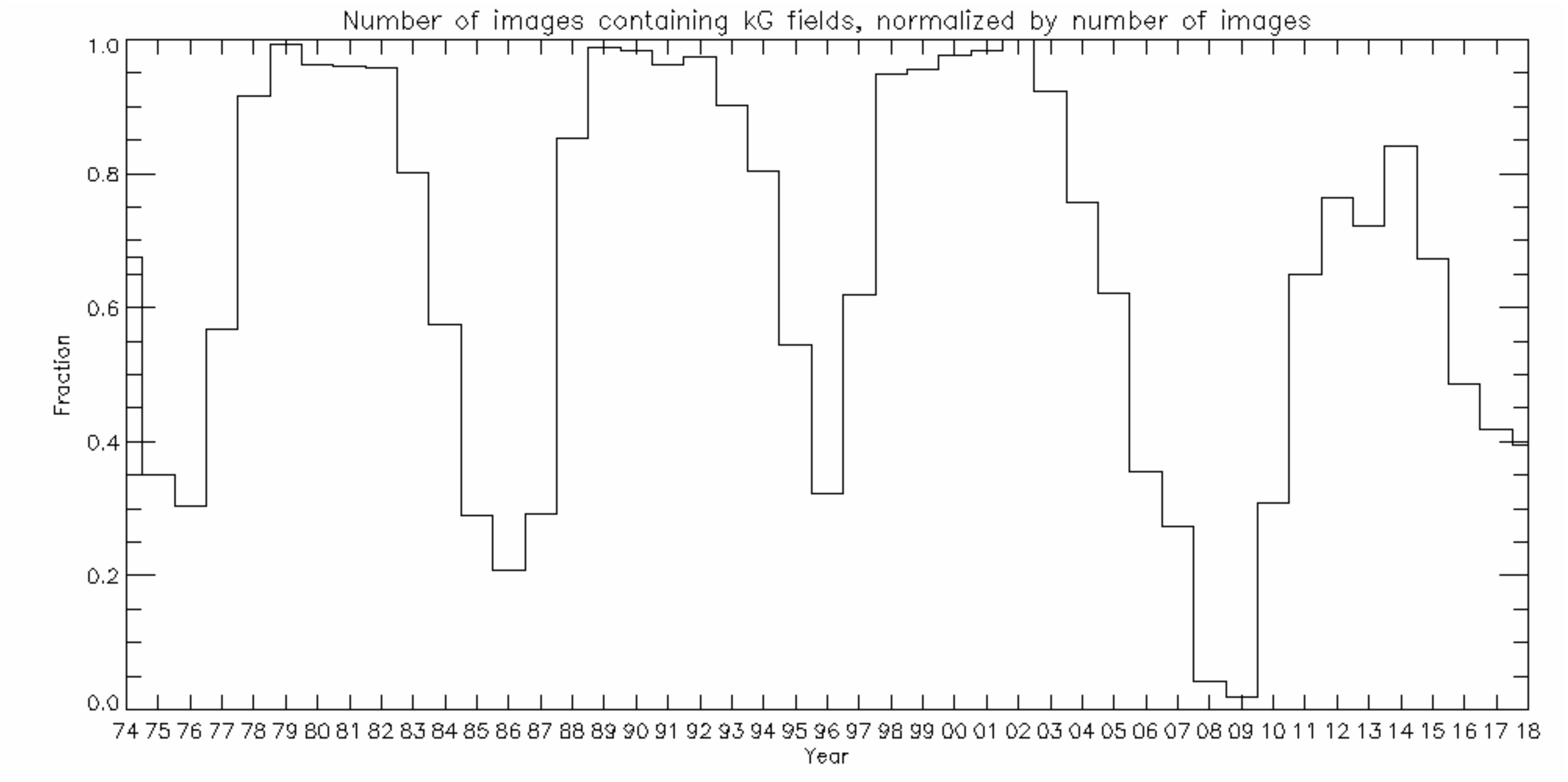

Active region flux centroids

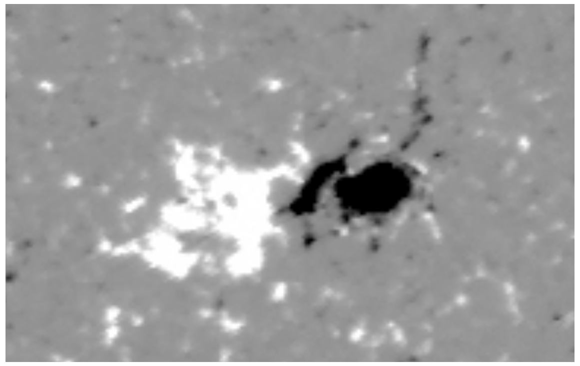

Solid: north hemisphere
dashed: south hemisphere

+ve flux
-ve flux

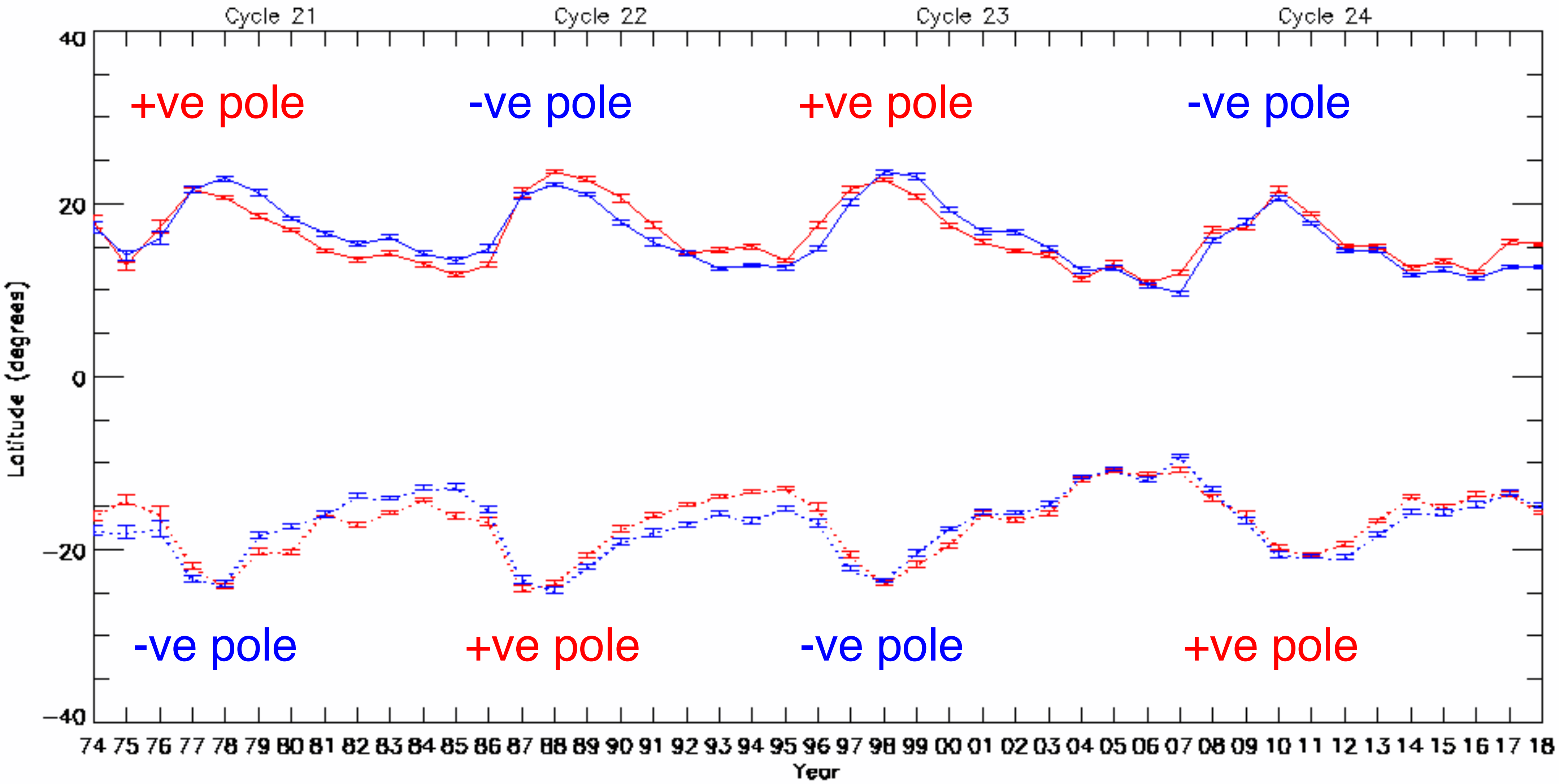

AR poloidal field opposes polar dipole at beginning of each cycle and remains until end of cycle through polar reversal – apart from decline of cycle 23 (Petrie 2012, Jiang et al. 2015).

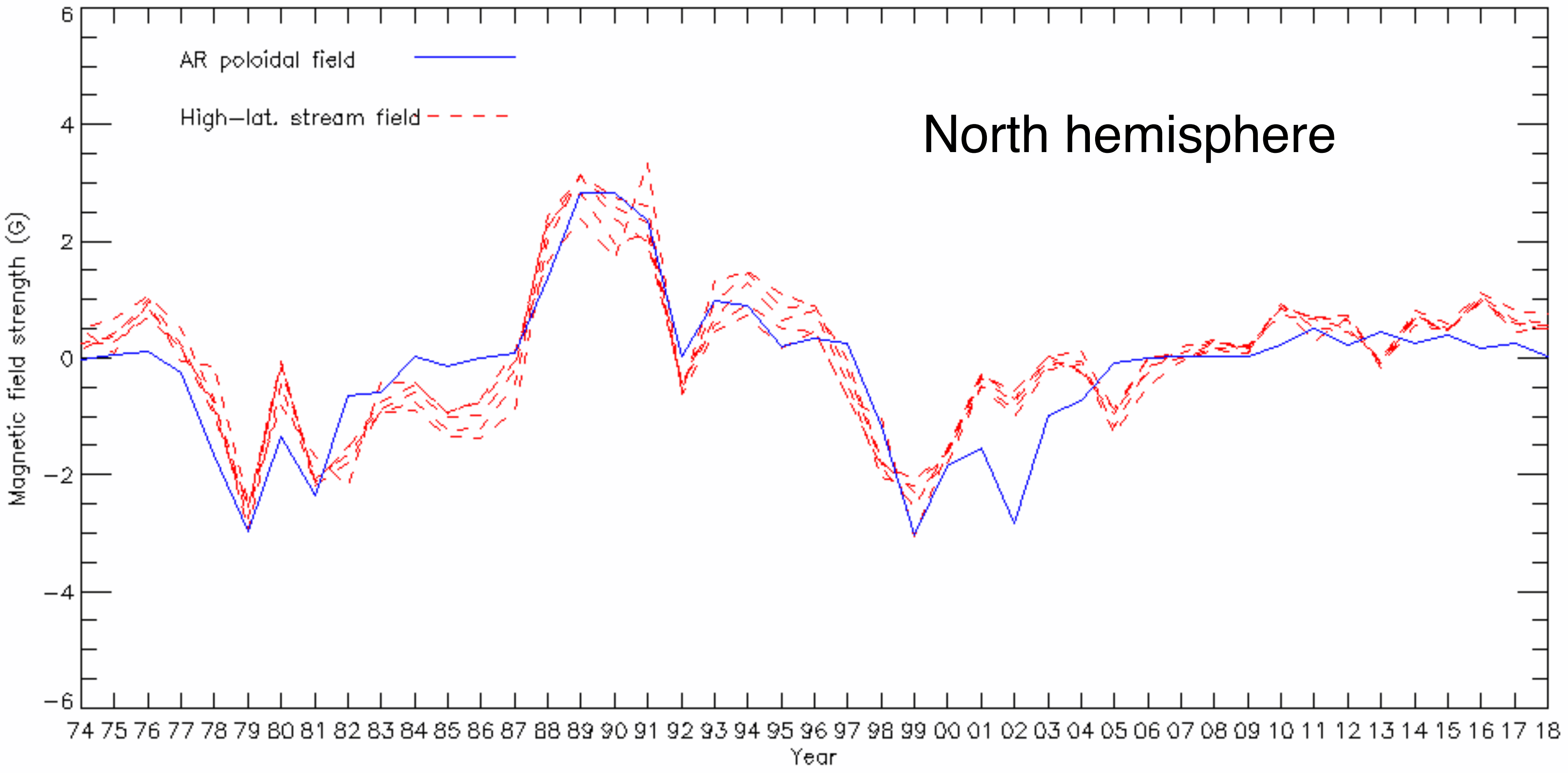

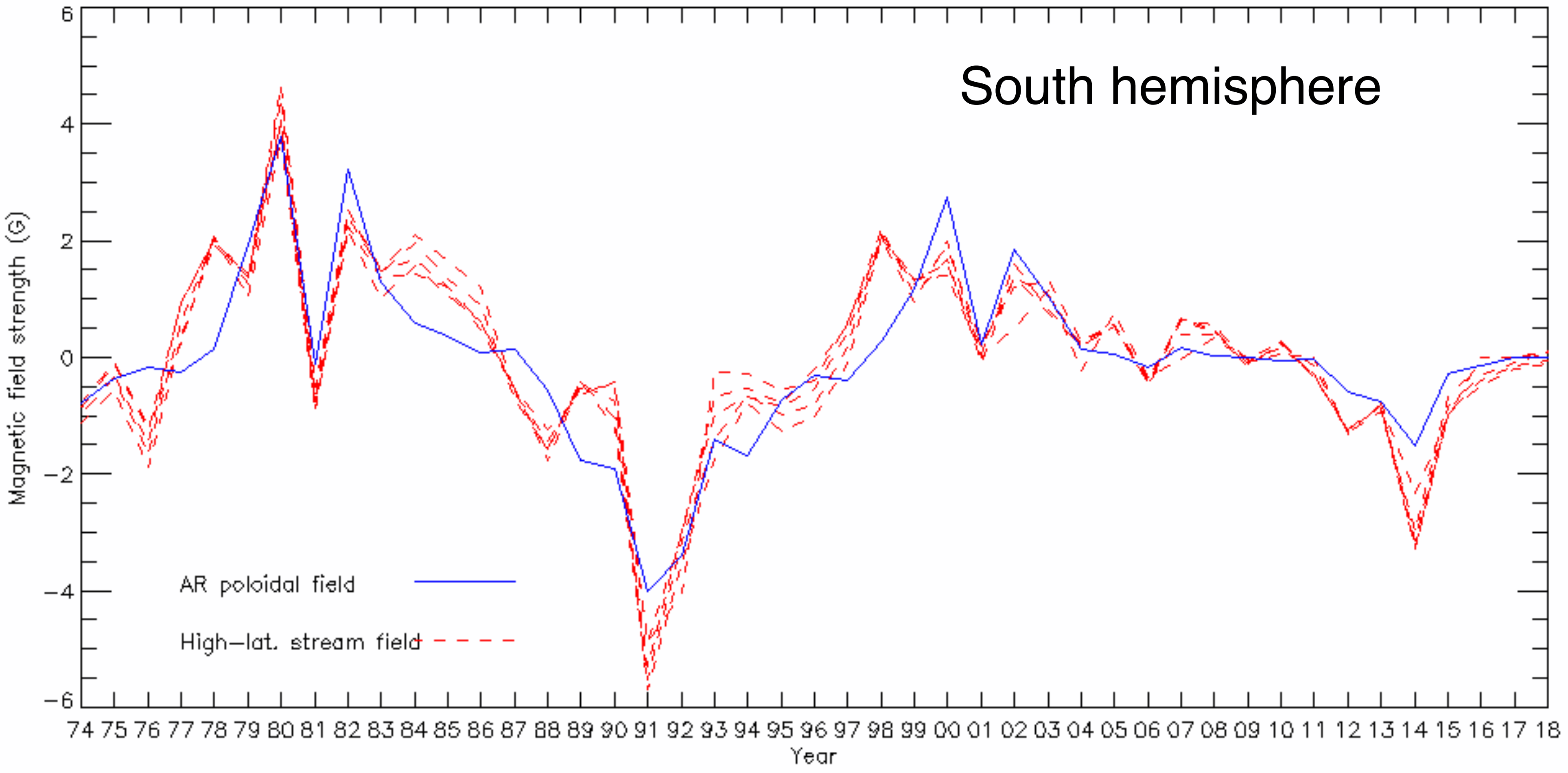

High-latitude stream field strength compared to AR total flux * centroid displacement/ area

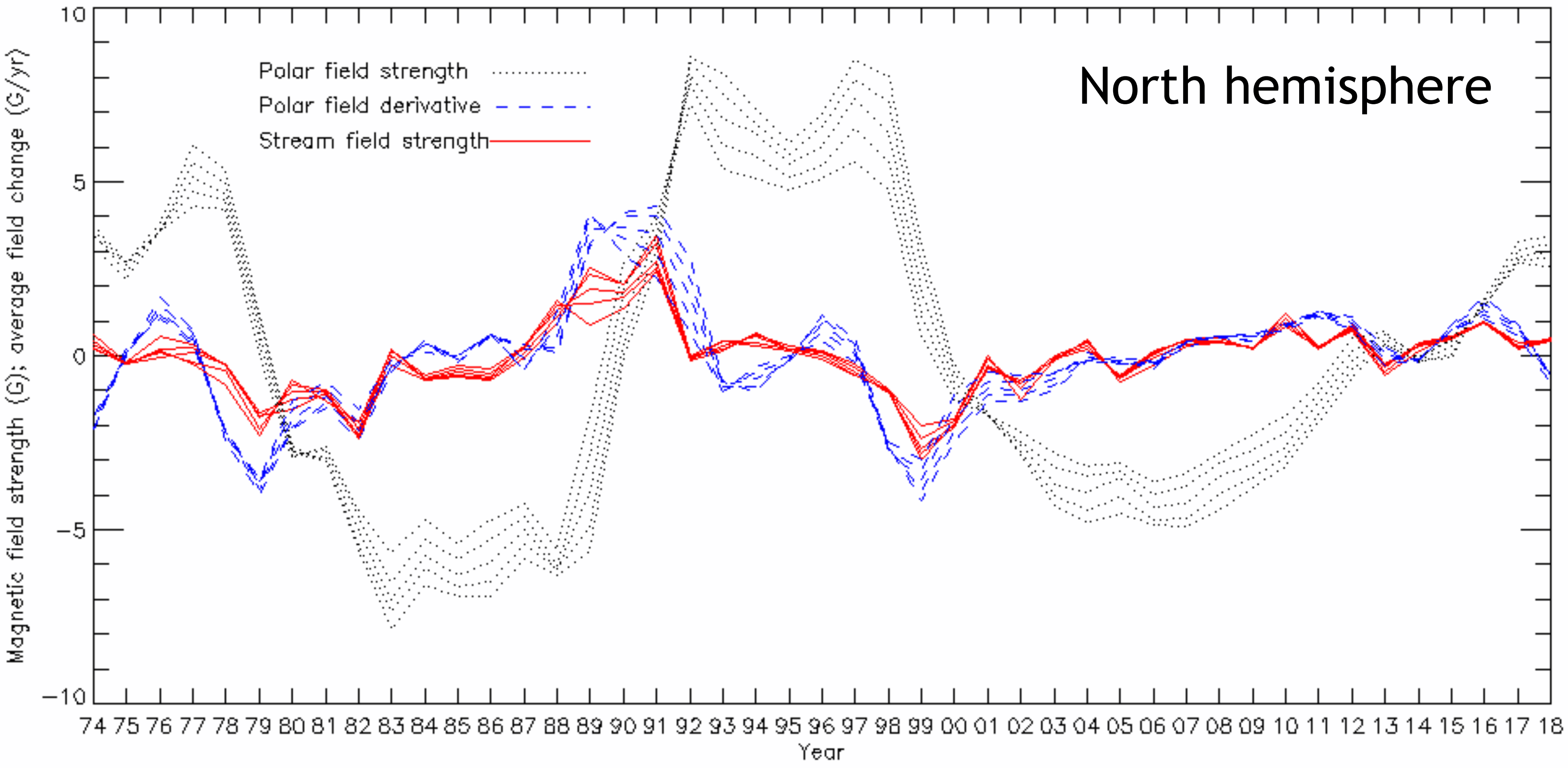

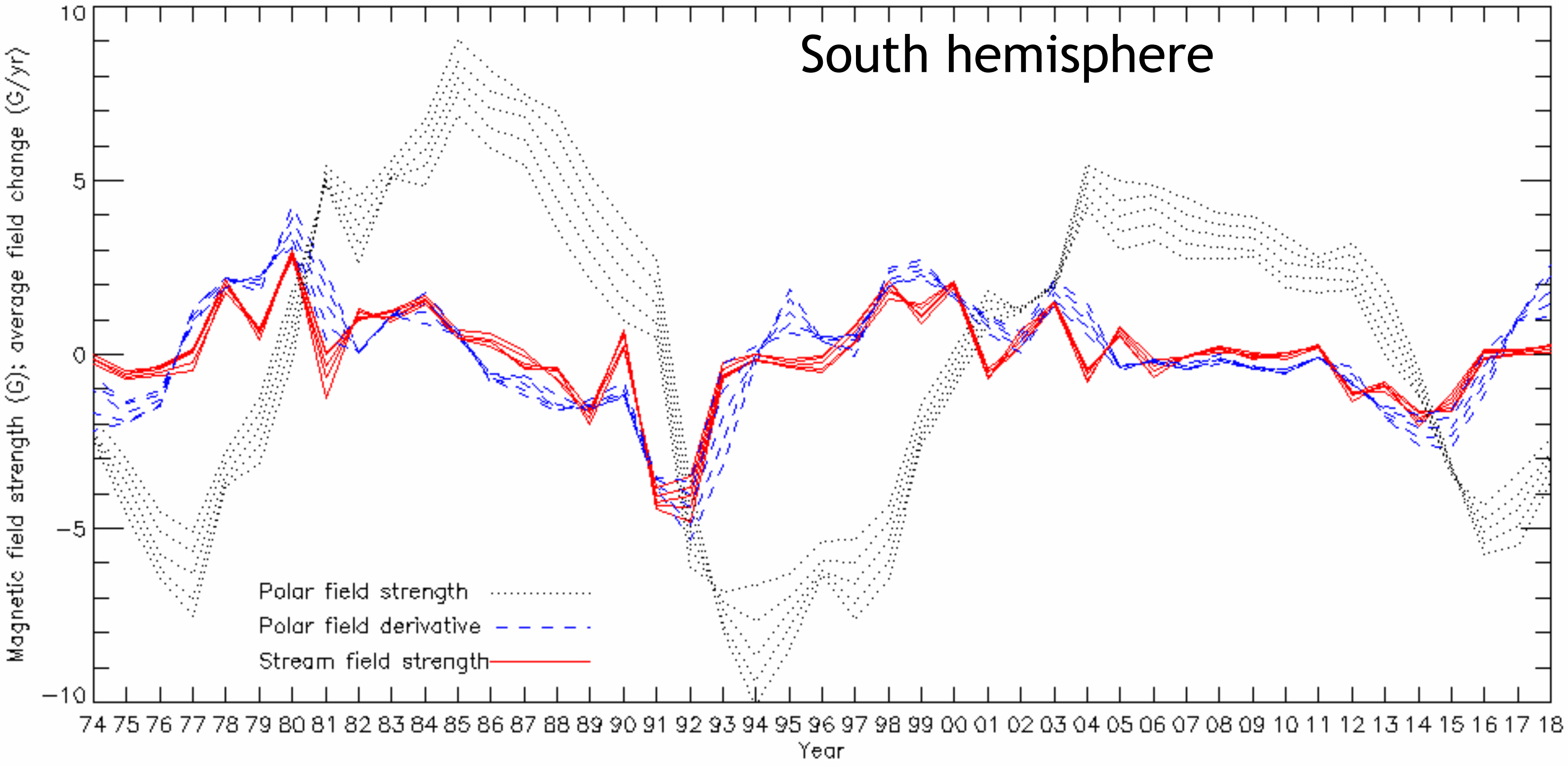

High-latitude stream field strength compared to polar field time-derivative

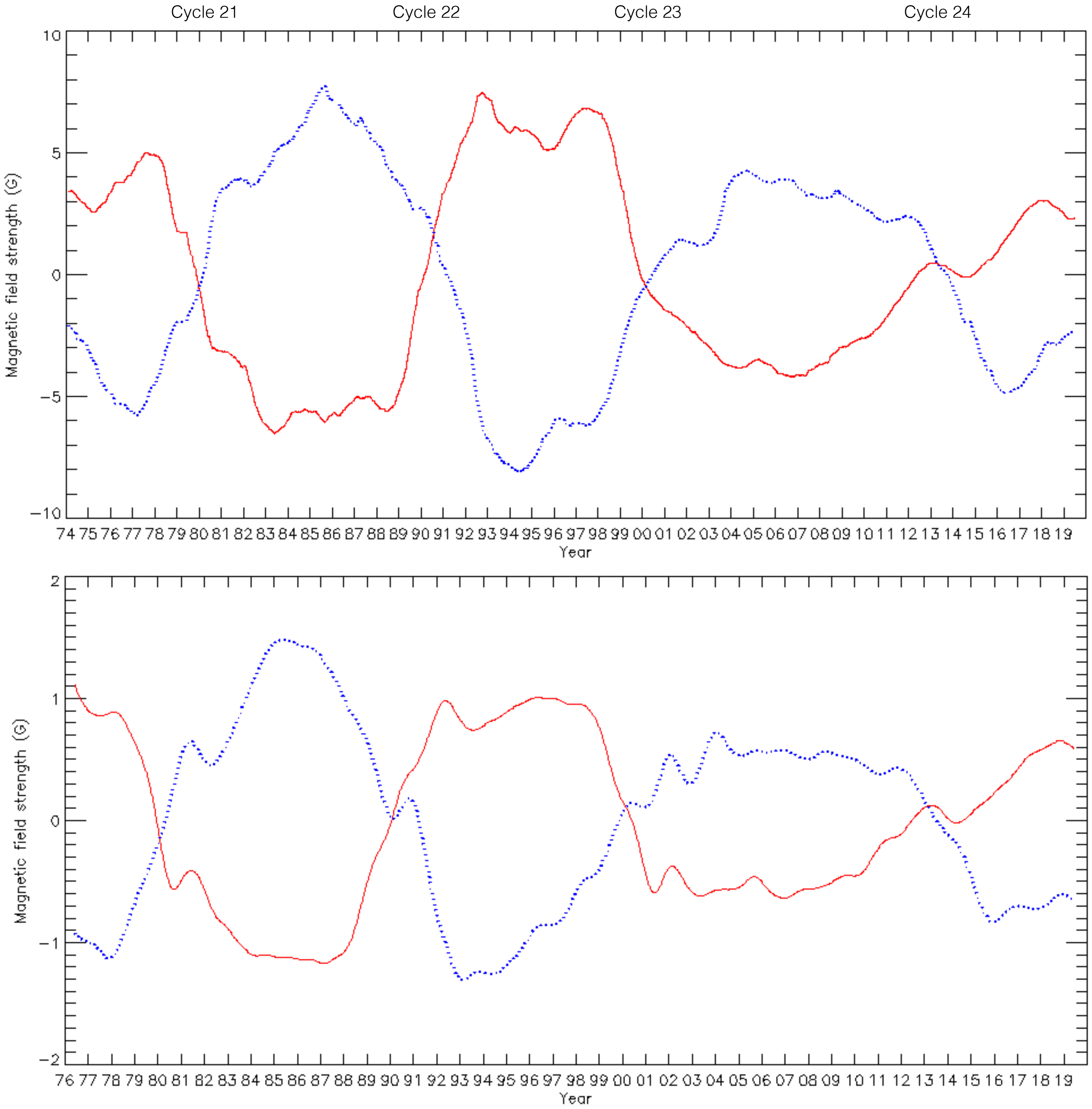

Cyclical polar field reversals

The north (red solid lines) and south (blue dotted lines) polar fields measured by NSO & HMI (from ±65°, top) and Wilcox (from ±55° to the poles, bottom) are plotted against time.

Cycle 23 polar fields only 60% as strong as previous two cycles.

Cycle 24: the north polar field reversed earlier, then reversed two more times, appears close to peak strength. The south polar field reversed quickly.

NSO SOLIS/VSM and HMI mismatch at poles?

Polar fields: HMI compared with WSO

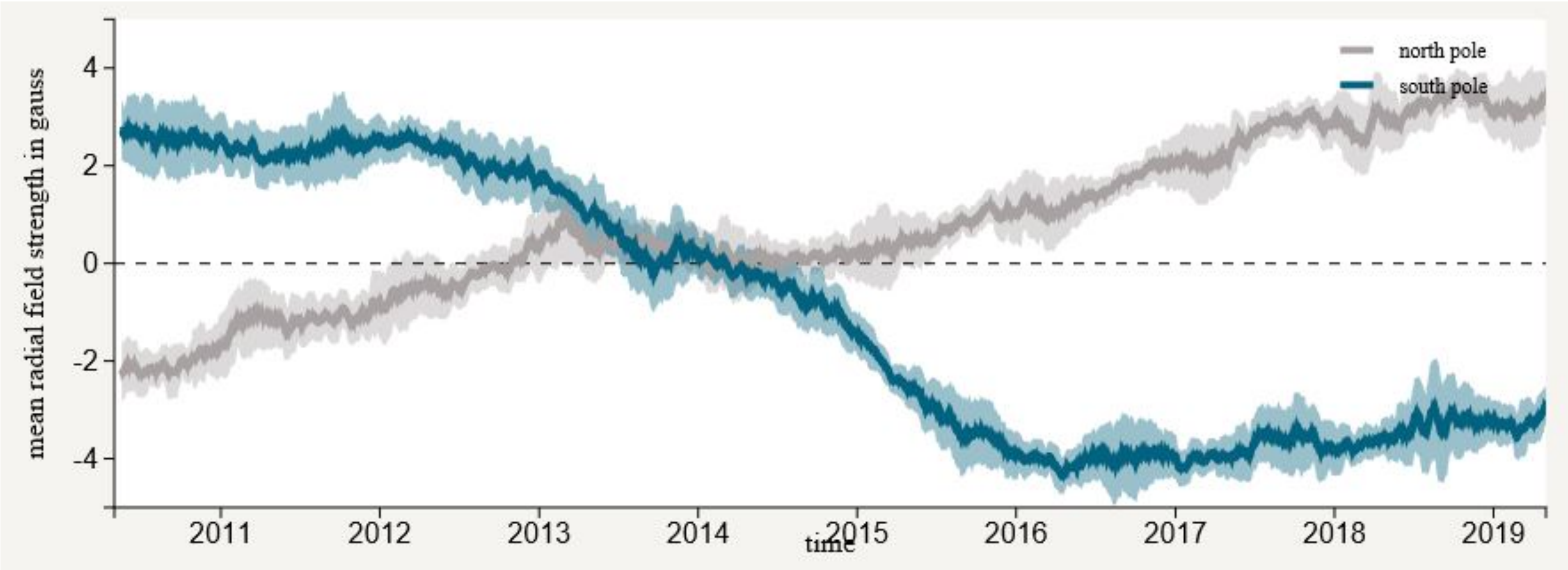

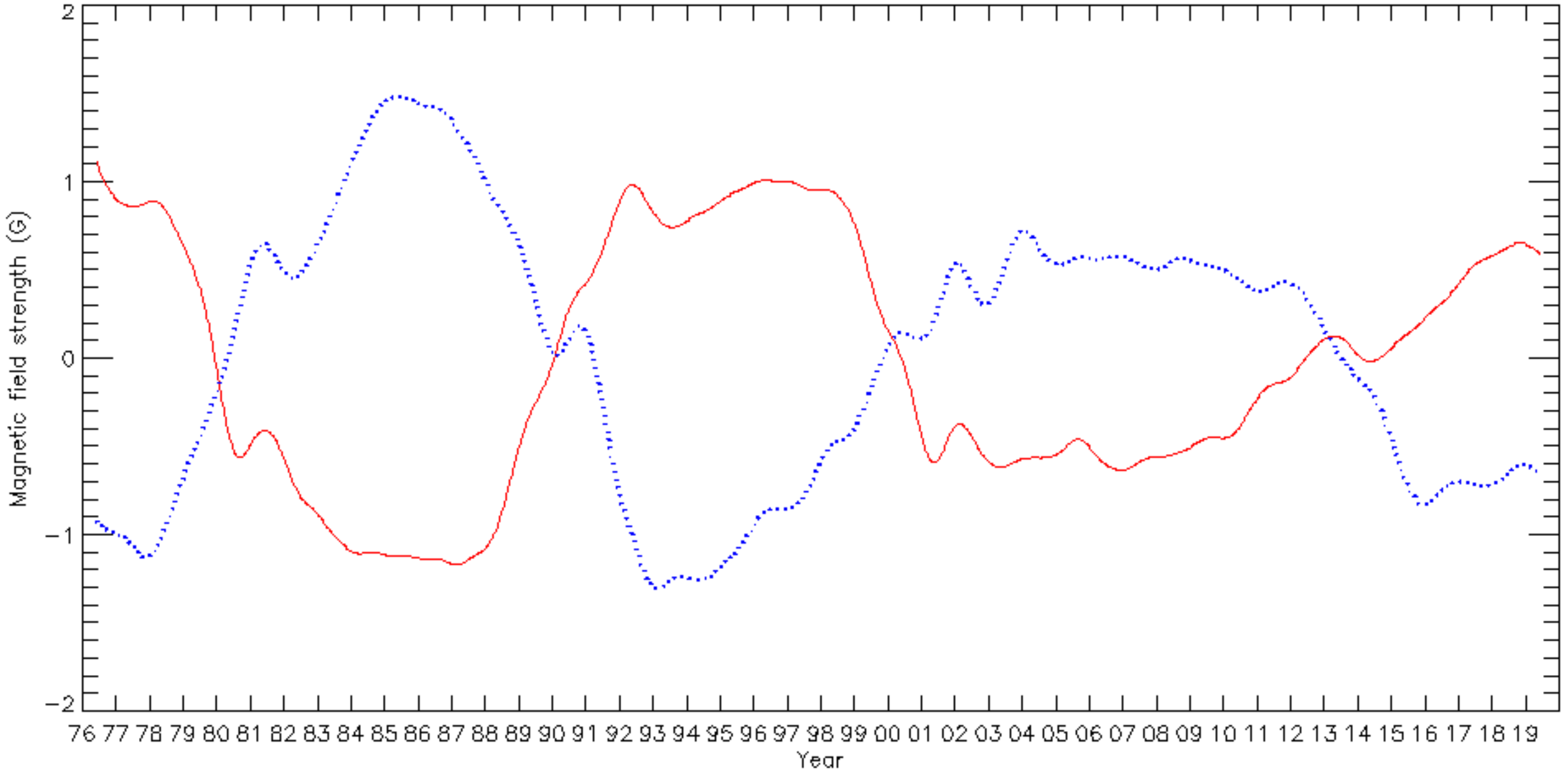

The north (red solid lines) and south (blue dotted lines) polar fields measured by HMI (top) and Wilcox (from ±55^{o} to the poles, bottom) are plotted against time.

WSO and HMI qualitatively agree.

Homework: cross-calibrate SOLIS/VSM and HMI all the way to the poles.

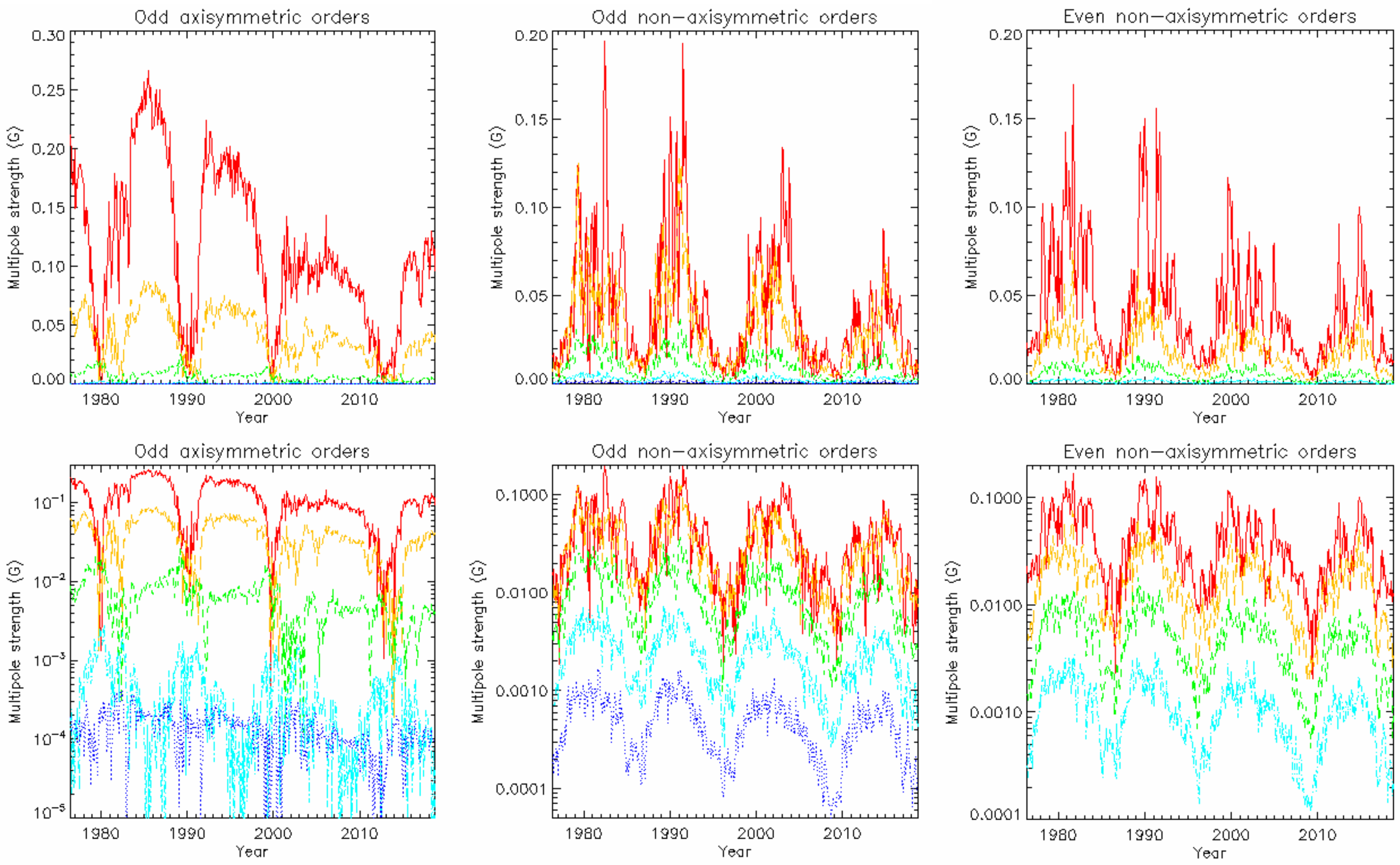

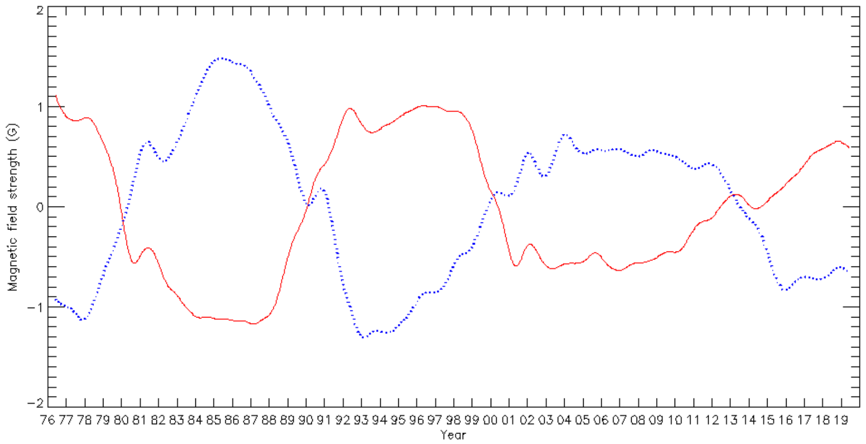

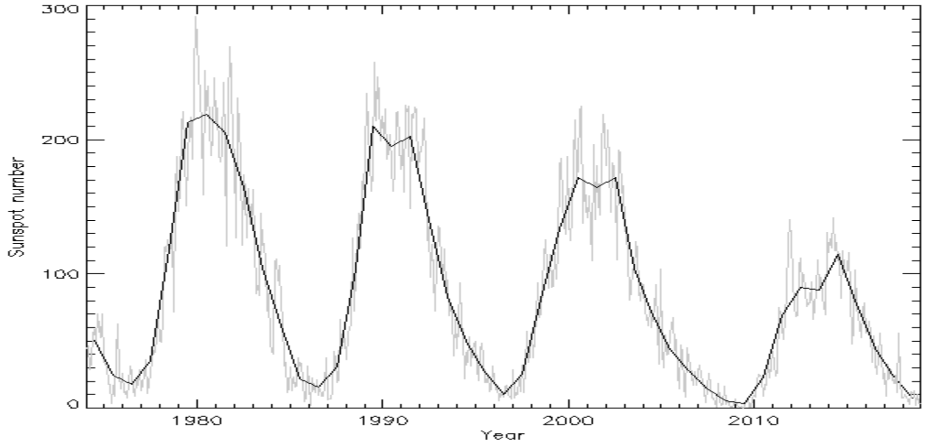

Wilcox data: for odd orders, red, amber, green, cyan and blue represent orders n=1, 3, 5, 7, 9. For even orders, red, amber, green and cyan represent orders n=2, 4, 6, 8.

Orders higher than n=4 correlate well (cc≈0.96) with the sunspot number. The low-order even multipoles also correlate well (cc>0.9) with the sunspot number.

Only the low-order odd axisymmetric (m=0) multipoles, the dipole (n=1, cc=0.97) and octupole (n=3, cc=0.96), follow the polar fields, but they are dominant over most of the cycle.

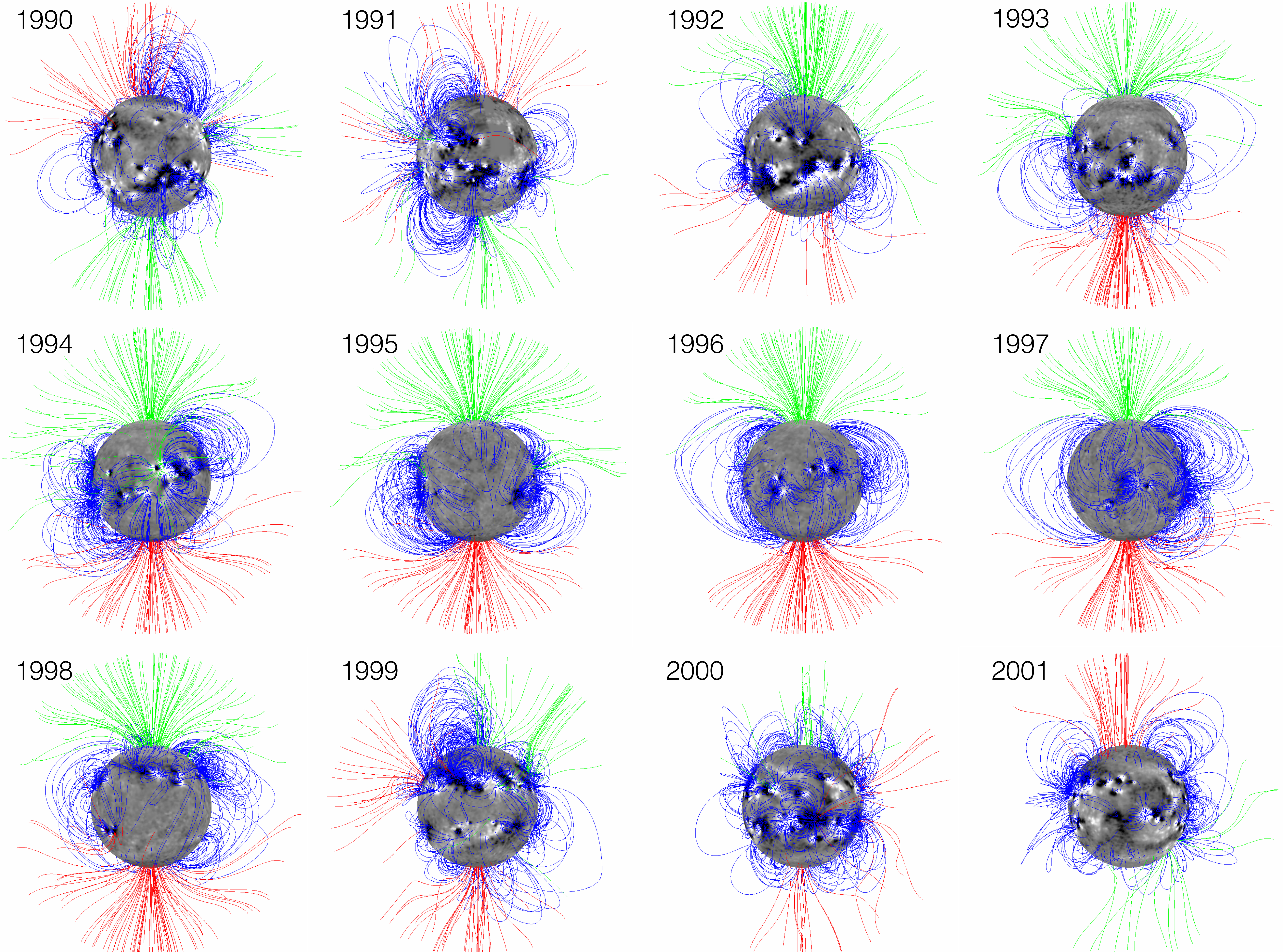

PFSS solutions computed using NCAR MUDPACK elliptic PDE solver and NSO synoptic data.

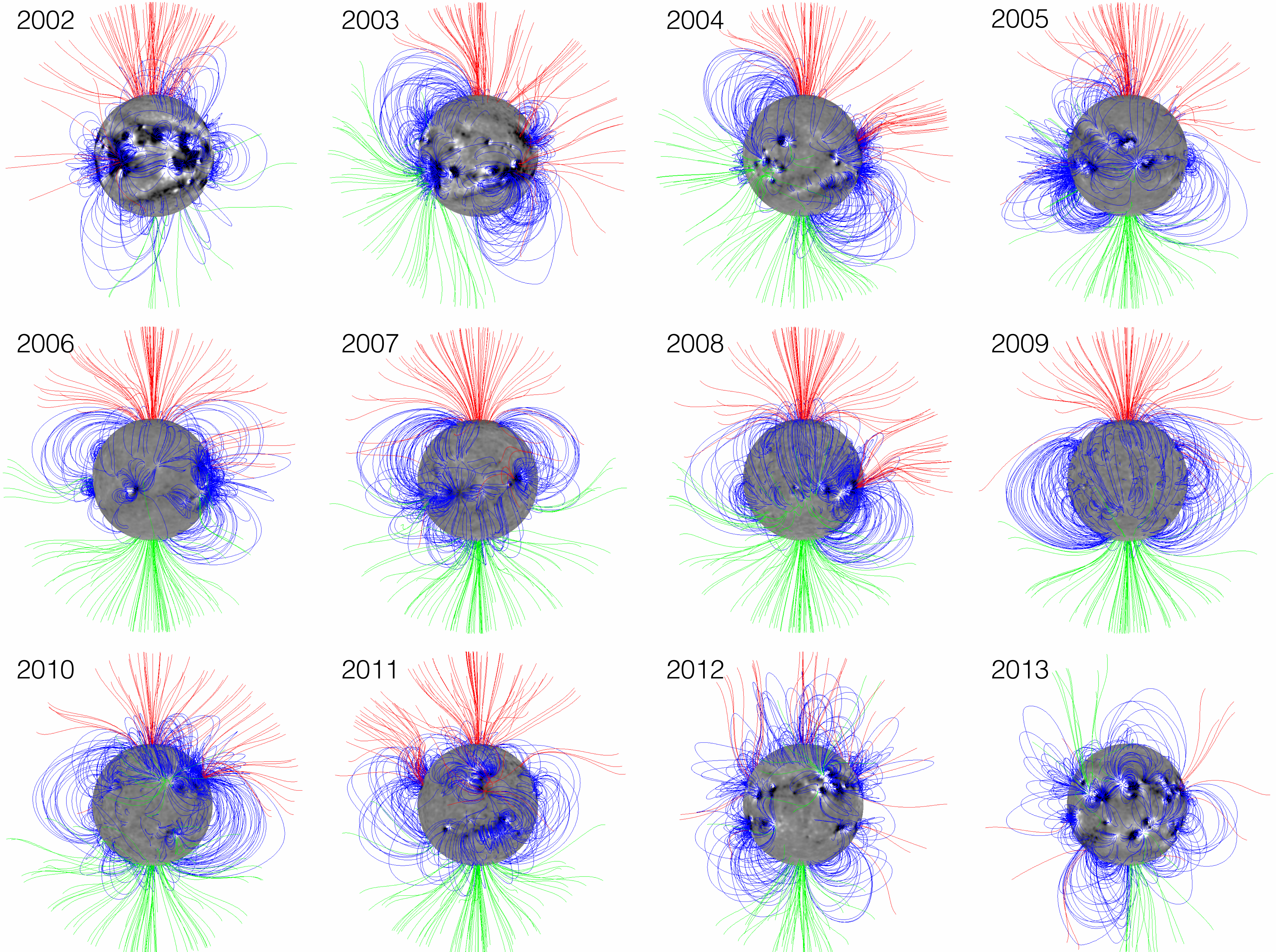

PFSS solutions computed using NCAR MUDPACK elliptic PDE solver and NSO synoptic data.

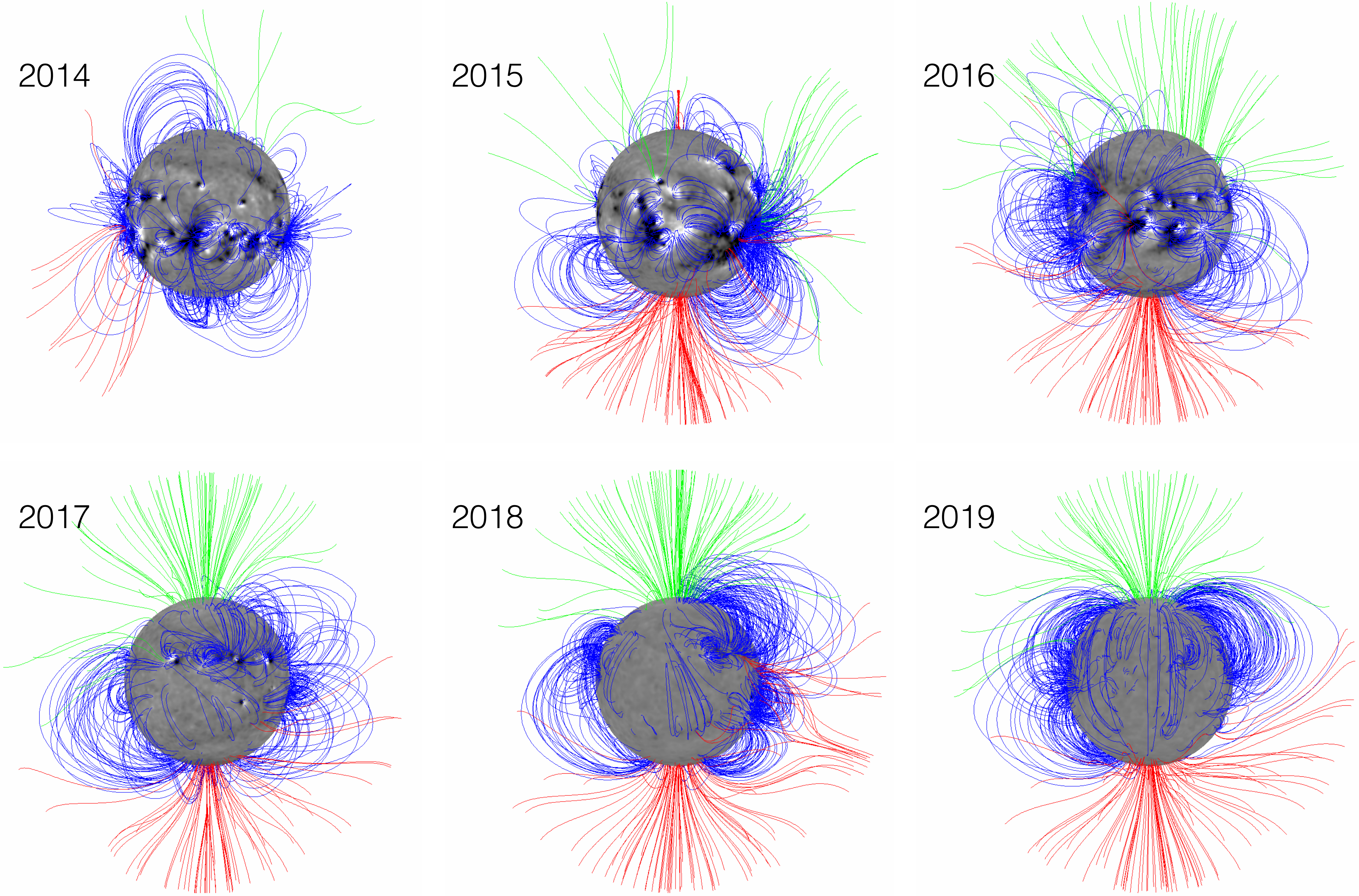

PFSS solutions computed using NCAR MUDPACK elliptic PDE solver and SOLIS/VSM synoptic data.

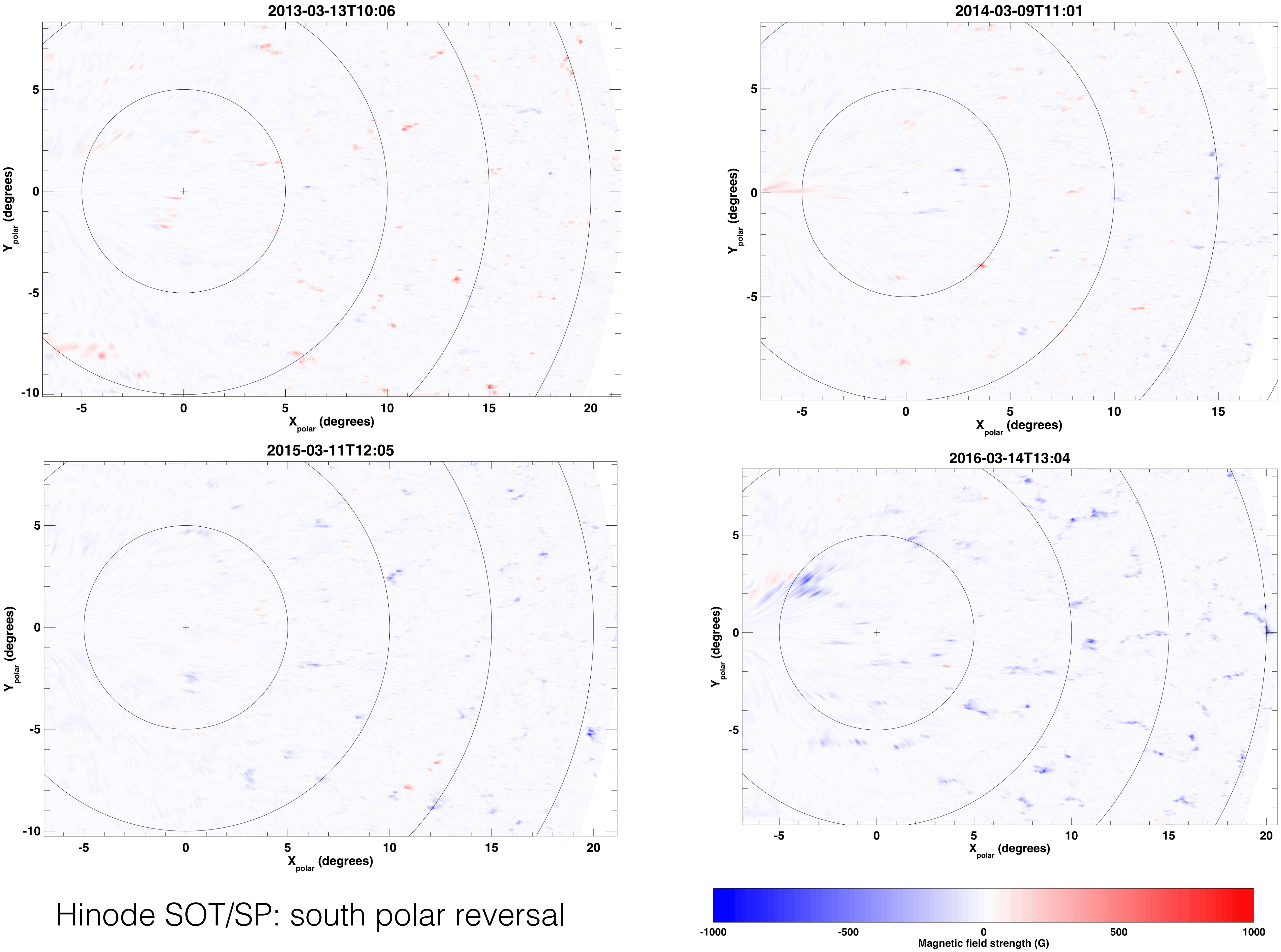

Hinode SOT/SP: south polar reversal

Hinode SOT/SP: south polar reversal

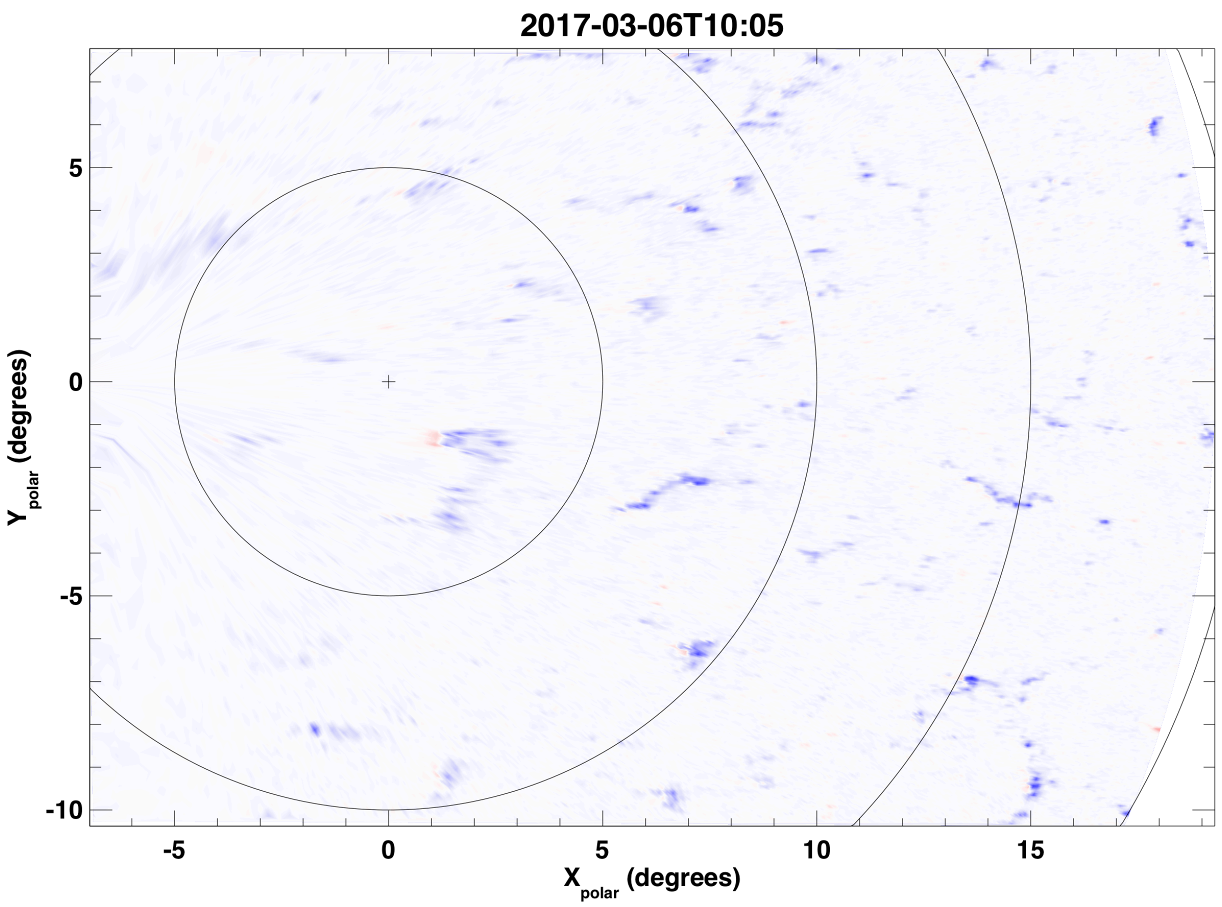

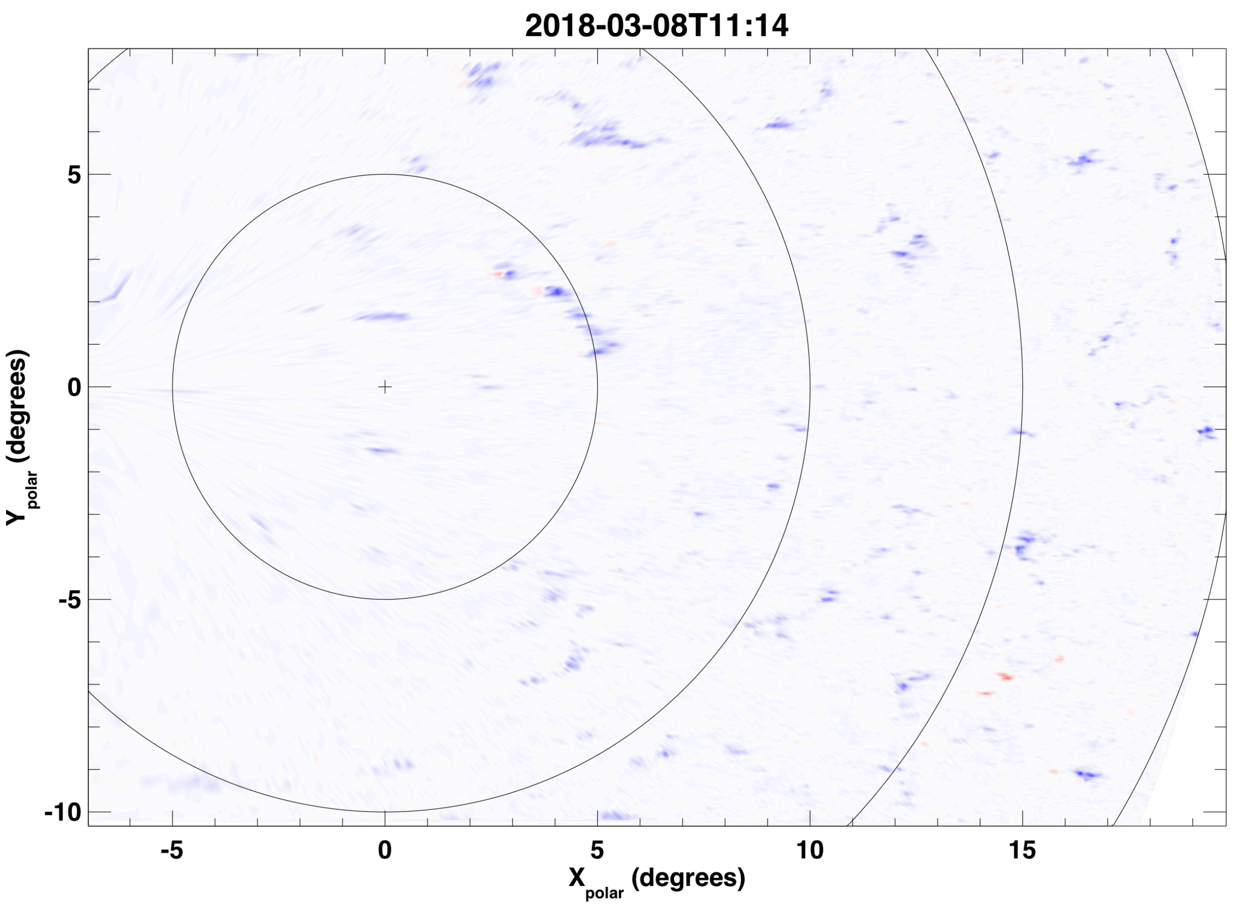

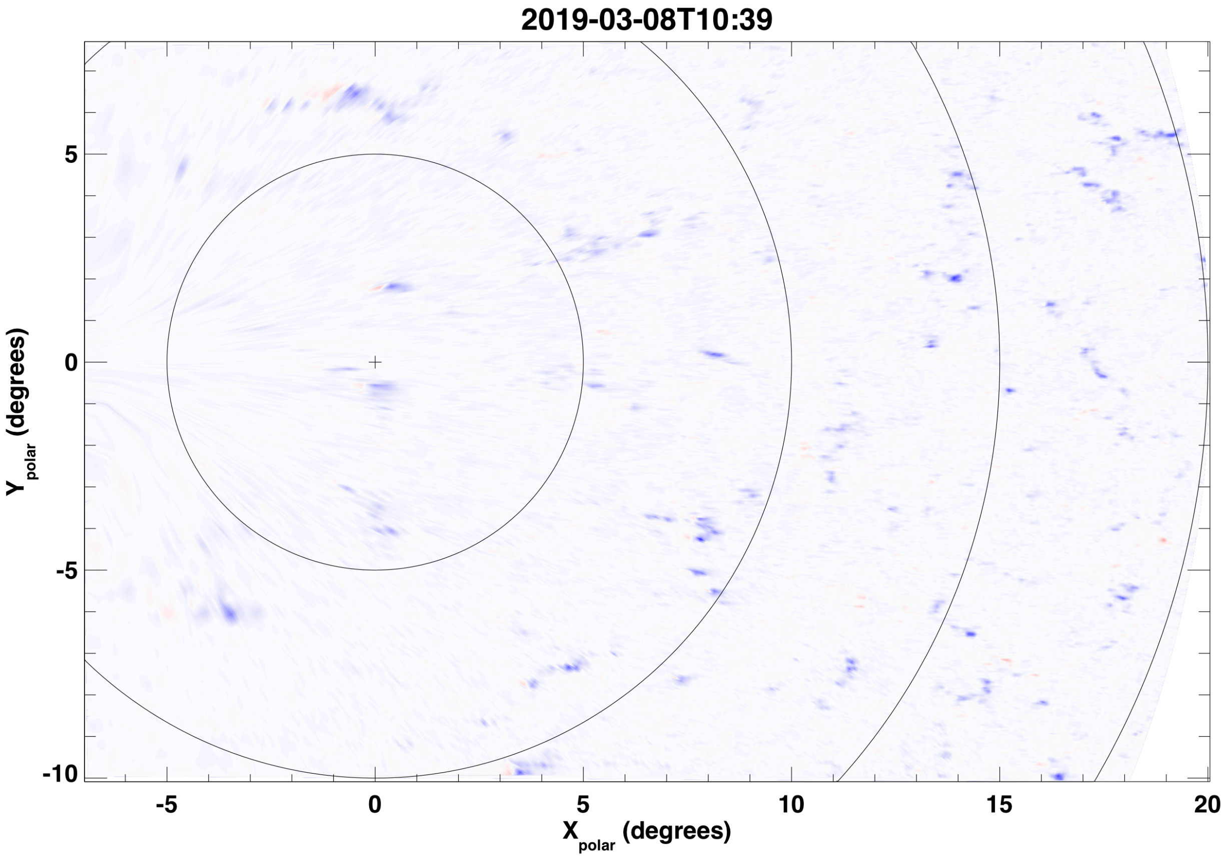

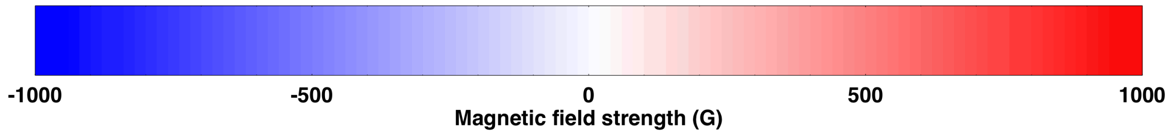

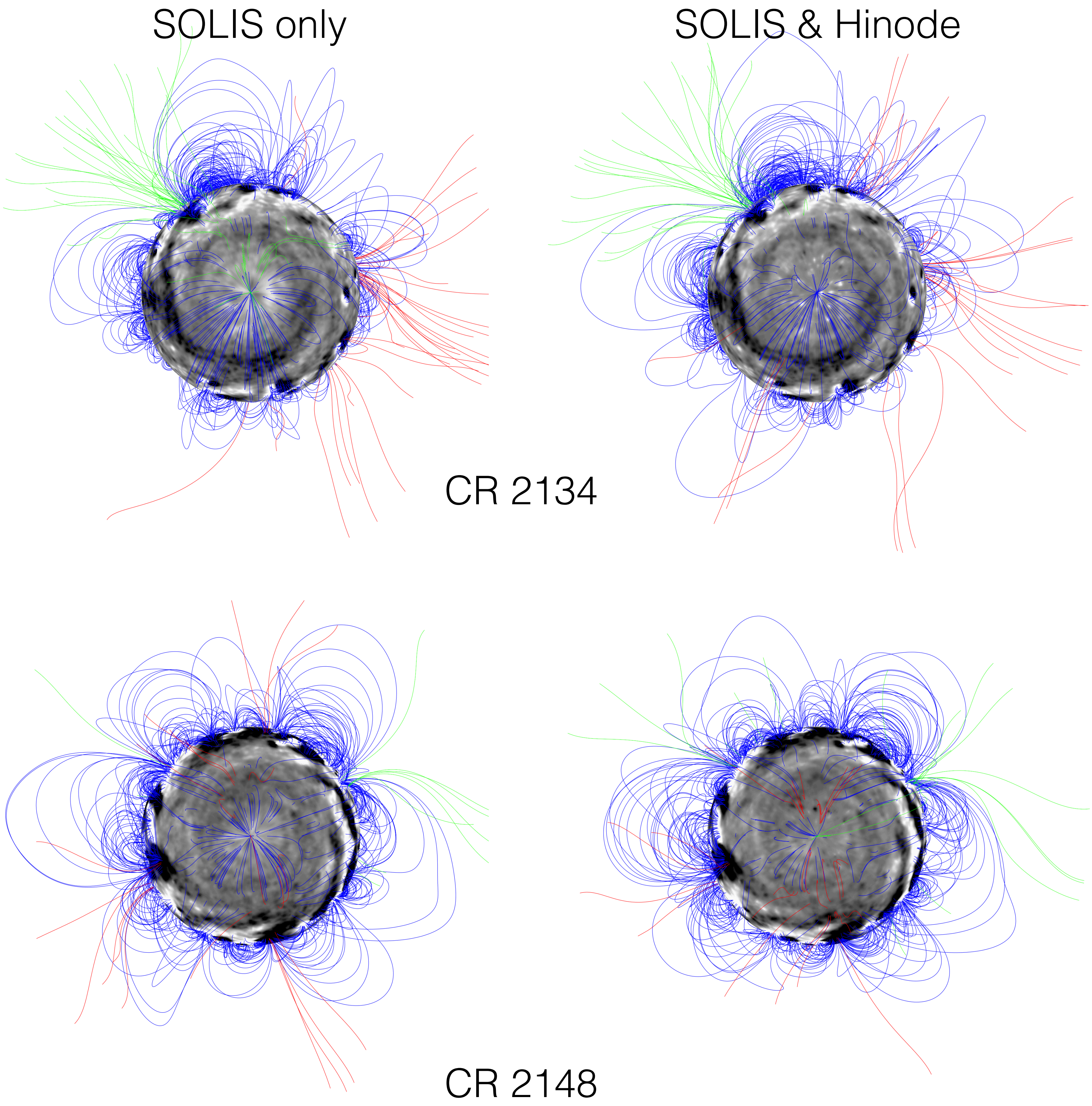

Polar projections of coronal PFSS field lines overplotted on magnetograms for CRs 2134 and 2148 from March 2013 and 2014, respectively.

Open positive/negative field lines are plotted green/red and closed field lines blue. The photospheric radial flux density is represented in greyscale saturated at ±10G with light/dark grey representing positive/negative flux density.

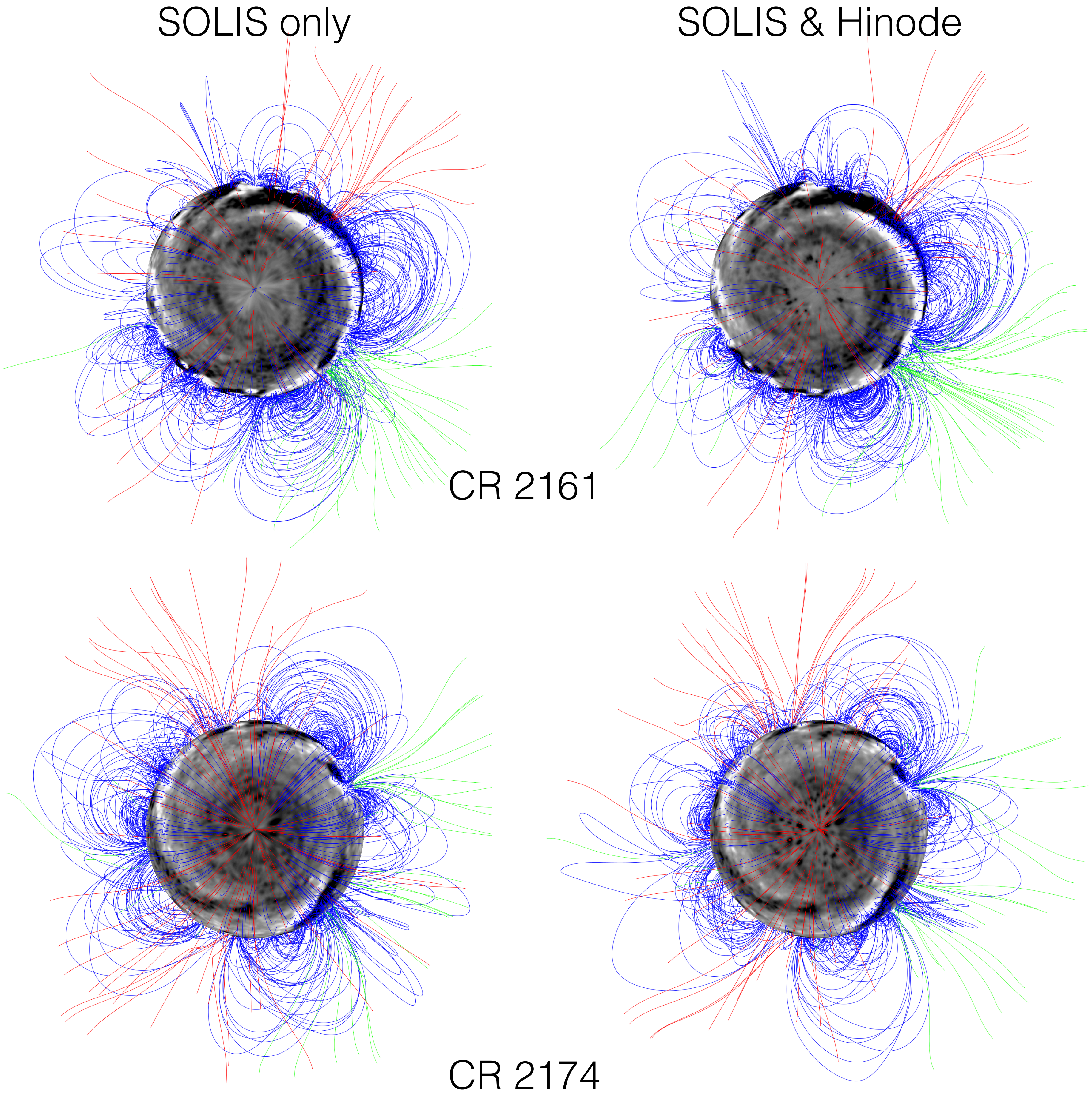

Polar projections of coronal PFSS field lines overplotted on magnetograms for CRs 2161 and 2174 from March 2015 and 2016, respectively.

Open positive/negative field lines are plotted green/red and closed field lines blue. The photospheric radial flux density is represented in greyscale saturated at ±10G with light/dark grey representing positive/negative flux density.

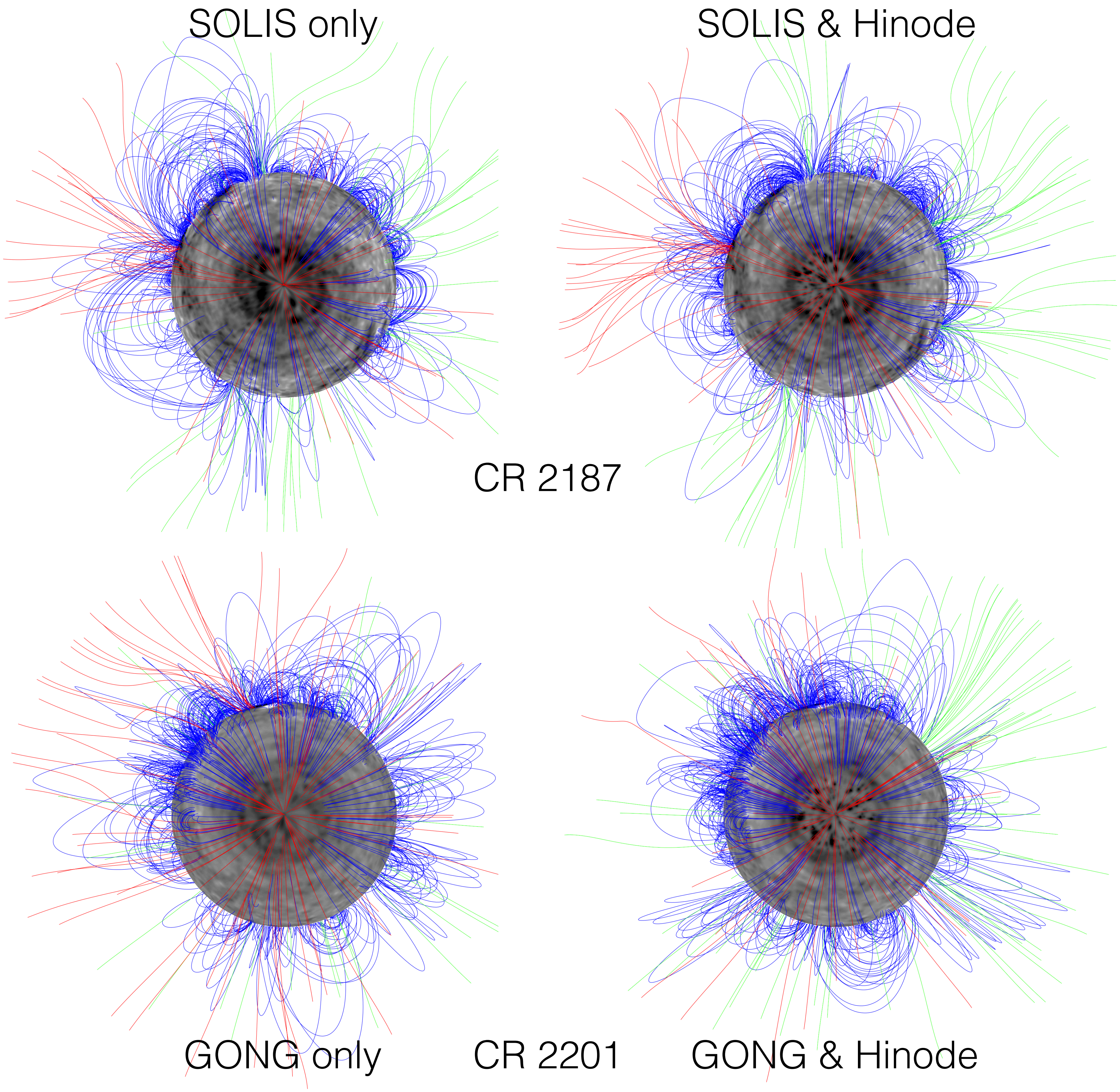

SOLIS only

SOLIS & Hinode

CR 2187

GONG only

CR 2201

GONG & Hinode

Polar projections of coronal PFSS field lines overplotted on magnetograms for CR s 2187 and 2201 from March 2017 and 2018, respectively.

Open positive/negative field lines are plotted green/red and closed field lines blue. The photospheric radial flux density is represented in greyscale saturated at ±10G with light/dark grey representing positive/negative flux density.

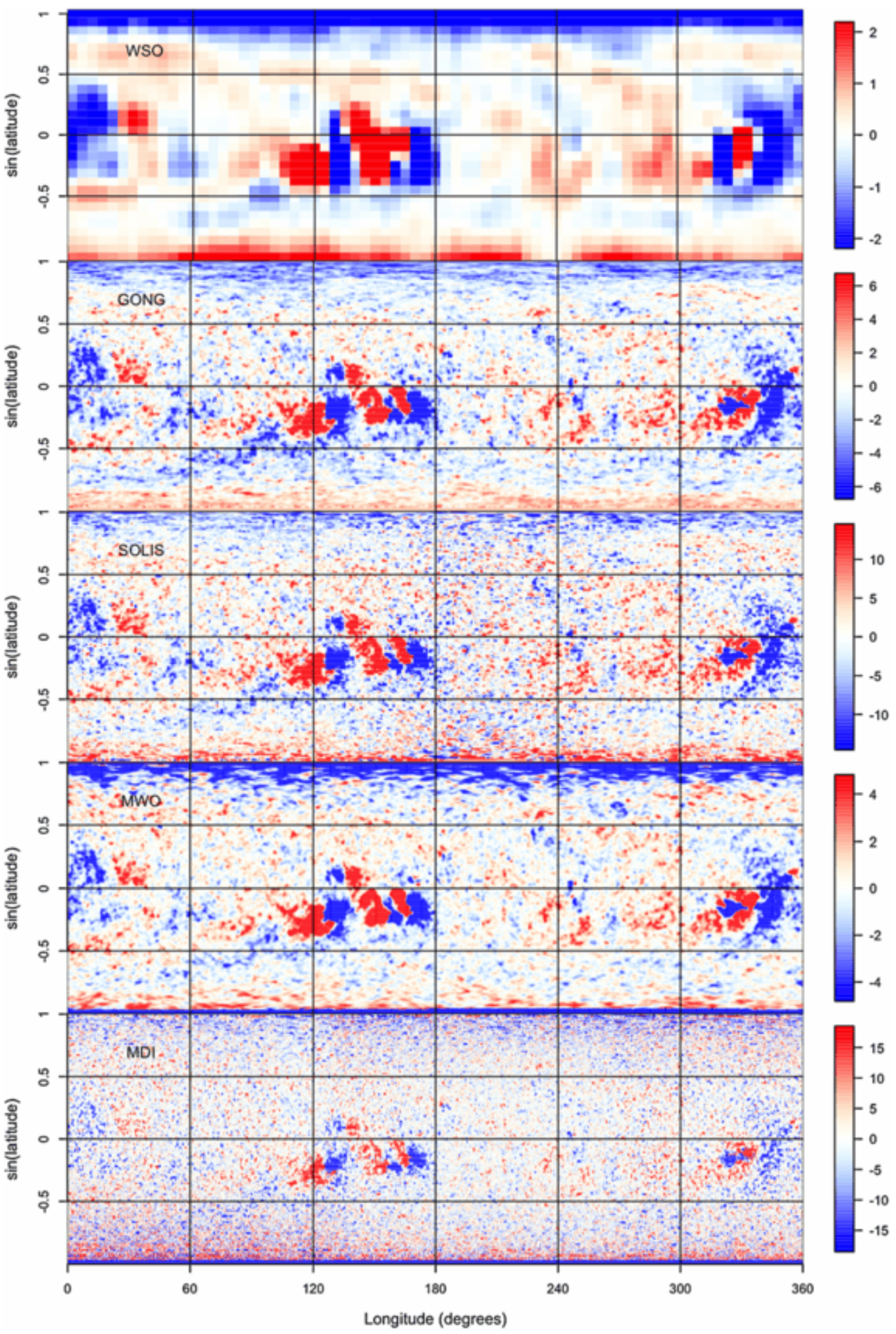

Problem with this work: different magnetographs measure different gauss.

Comparison of synoptic maps for five solar observatories for CR 2047. From top to bottom: Wilcox Solar Observatory (WSO); Global Oscillation Network Group (GONG); Synoptic Optical Long-term Investigations of the Sun (SOLIS), Mount Wilson Observatory (MWO); and Michelson Doppler Imager (MDI). All data are in their original resolution: WSO 73×30; GONG 360×180; SOLIS 360×180; MWO 971×512; and MDI 3600×1080.

From Riley et al. (2014).

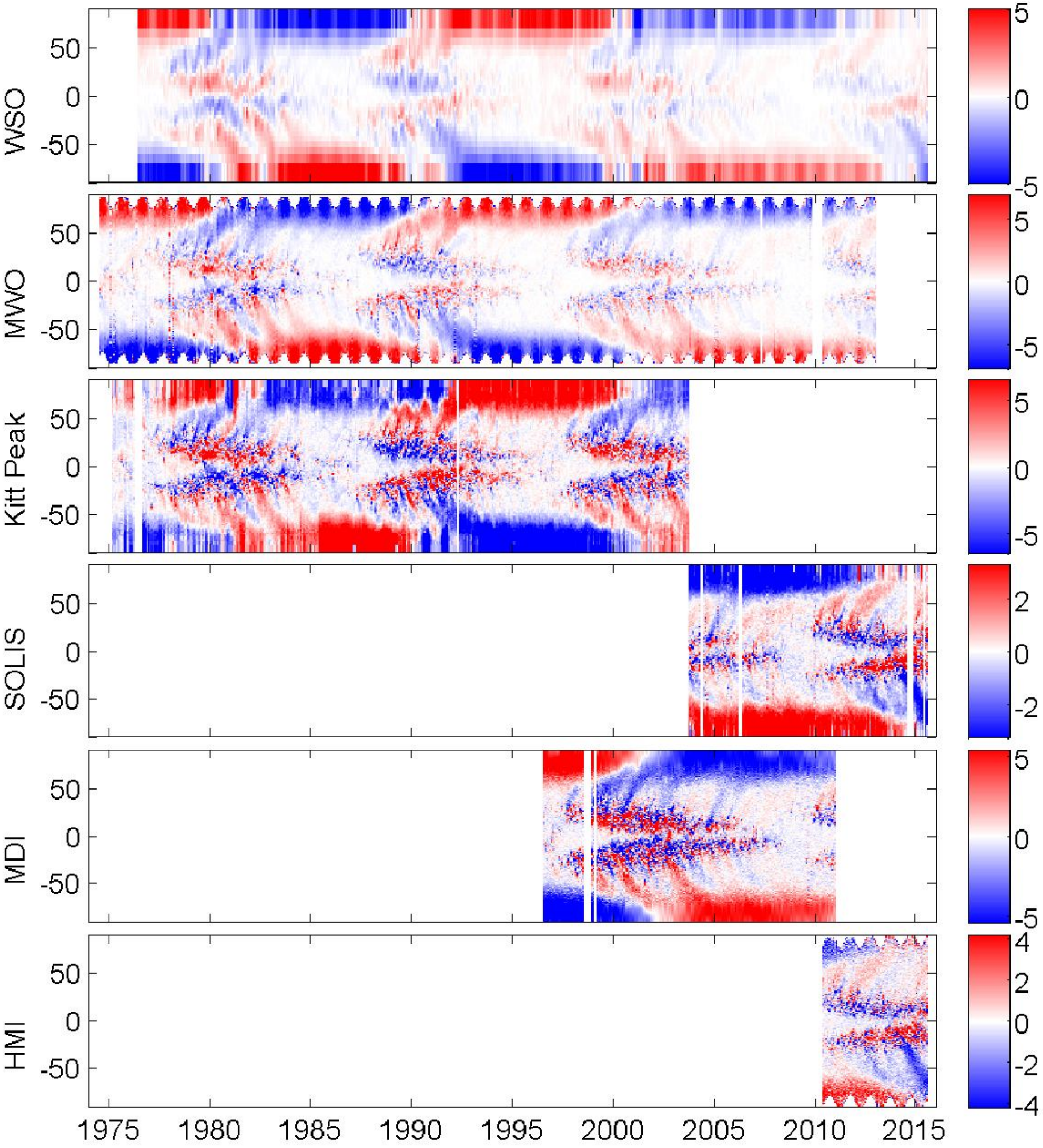

Latitude-time maps of the photospheric magnetic field six data sets. Color indicates the field intensity.

From Virtanen et al. (2016)

End-to-end Magnetogram Model

(with V. Martínez Pillet and J. Blanco Rodríguez)

We model the magnetogram observation from end to end, simulating the degradation of the signal from diffraction at the telescope aperture to the final inversion for the magnetic field.

Begin with known MHD (MURaM, Vögler et al. 2005) simulation data for the magnetic field as “ground truth”.

Compute spectra using radiative transfer code: Stokes Inversion with Response functions (SIR, Ruiz Cobo et al. 1992) code.

Use Solar Orbiter Polarimetric and Helioseismic Imager Software siMulator (SOPHISM, Blanco Rodríguez et al. 2018) to simulate the instrument response to emergent spectra (aperture diffraction, pixelization, GONG inversion for magnetic field, (noise, instrument polarization, etc.).

Compare simulated GONG magnetogram with MHD field data (weighted by response function).

J. Plowman (NSO) is developing a similar model using a different approach.

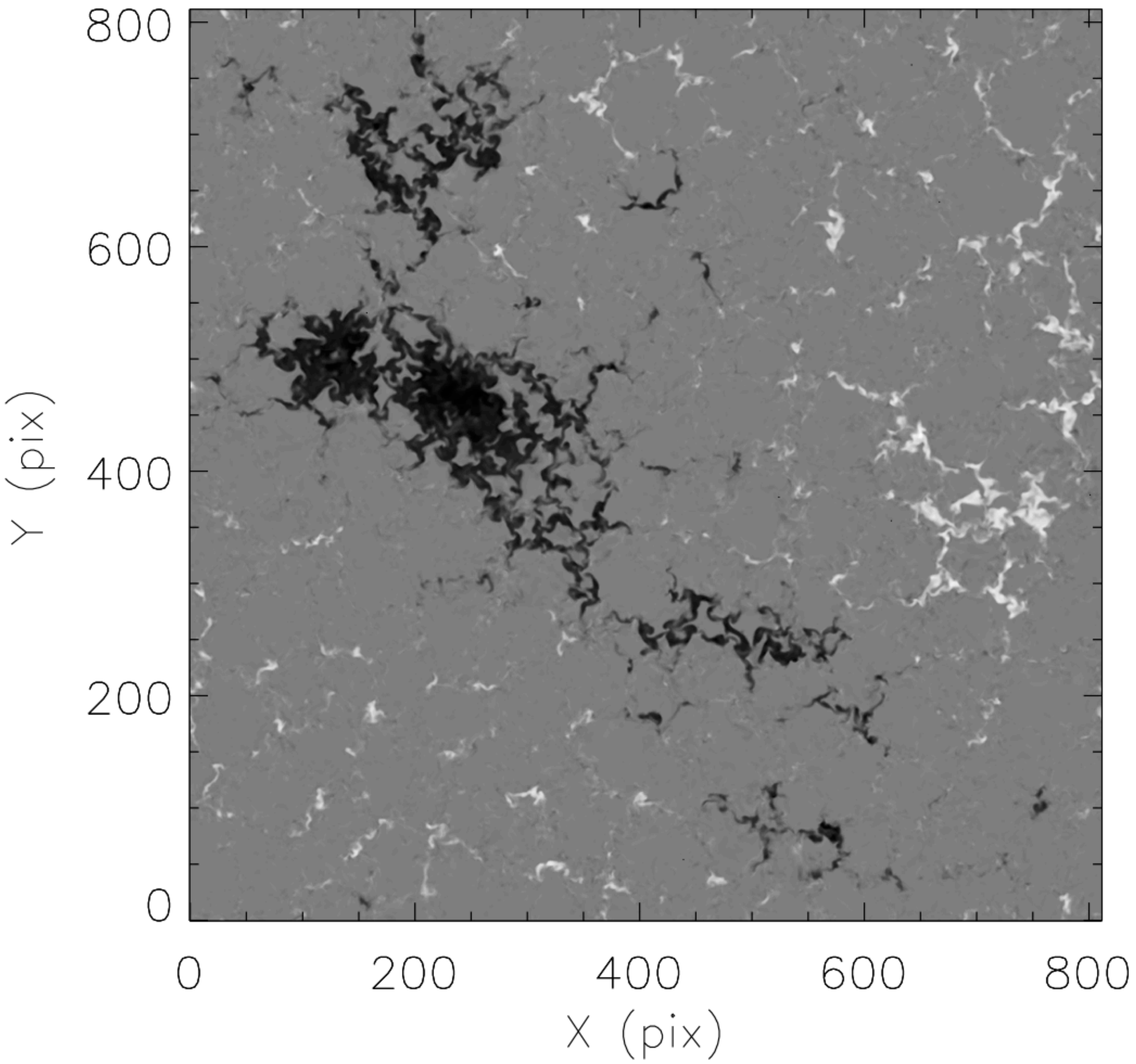

MURaM MHD simulation: 812 x 812 x 384 pixels, 41.7 km x 41.7 km x 16 km sampling.

Stokes (I,Q,U,V) spectra are computed from the MHD data cubes with SIR (Ruiz Cobo et al. (1992): 6768 Å ± 0.5 Å, 101 wavelengths,10 mÅ sampling.

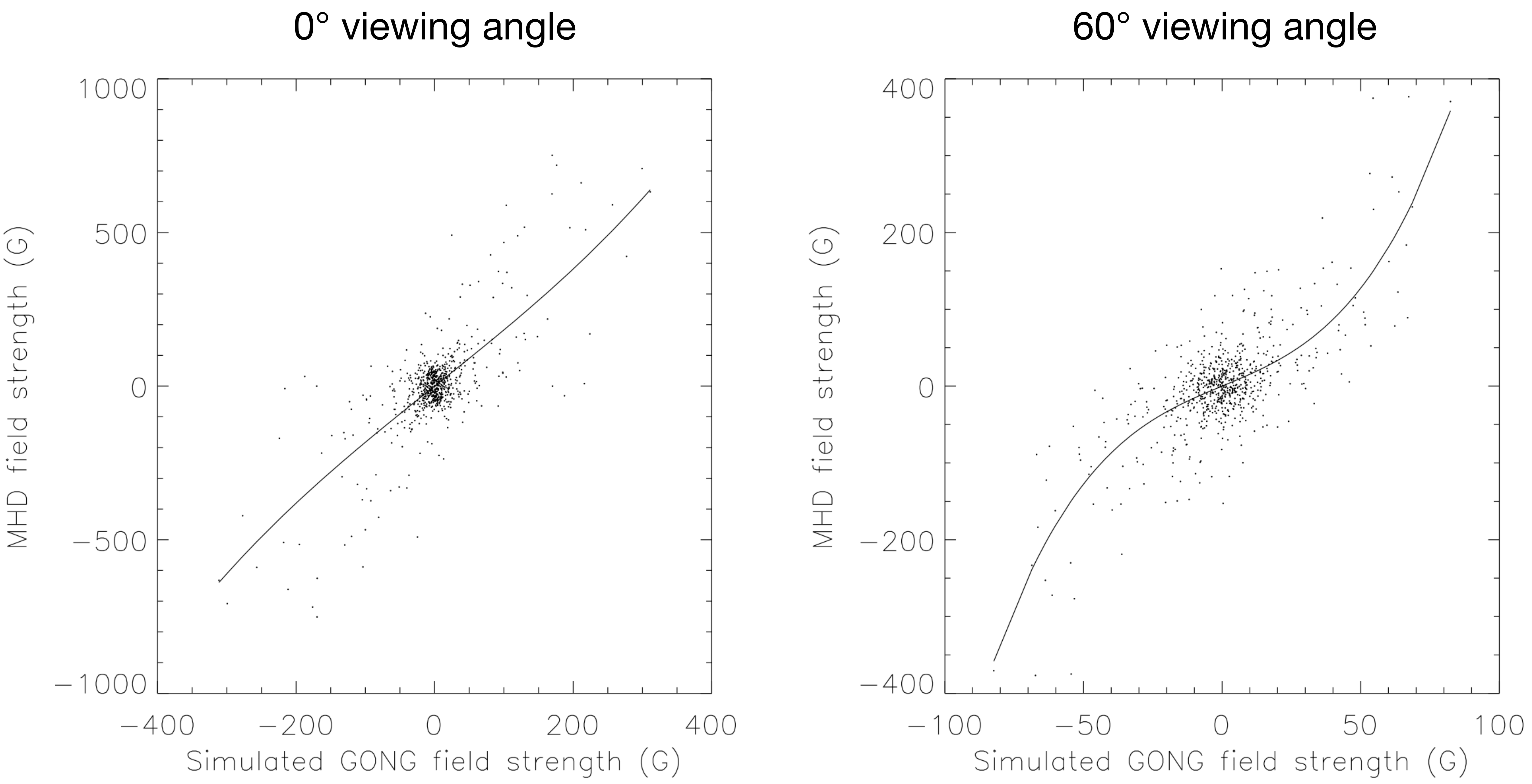

0° viewing angle

60° viewing angle

MHD field strength against simulated GONG field strength for cases with 0° (left) and 60° viewing angle (right).

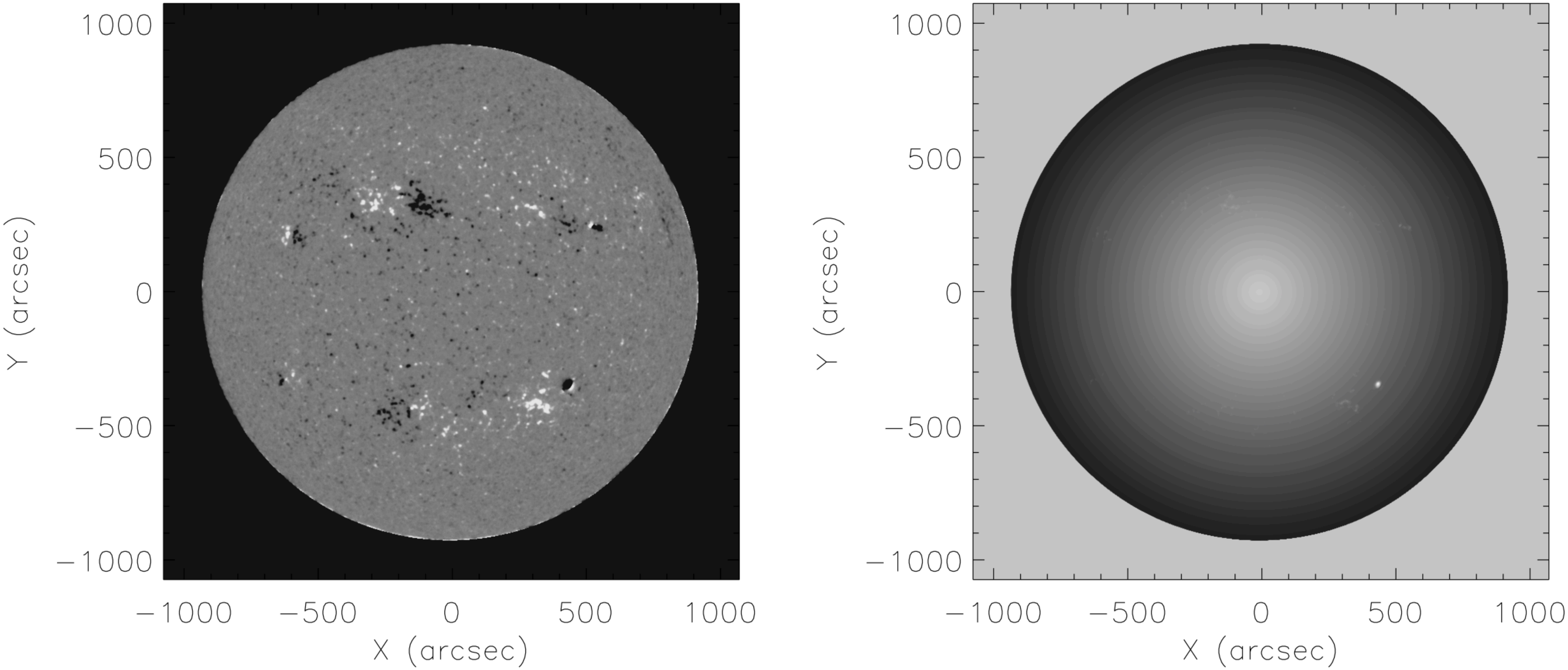

GONG magnetogram from 4 July 2010 saturated at ±50G (left) and associated calibration factor map (right). Calibration factor ranges from 1.4 (black) to 1.9 (white).

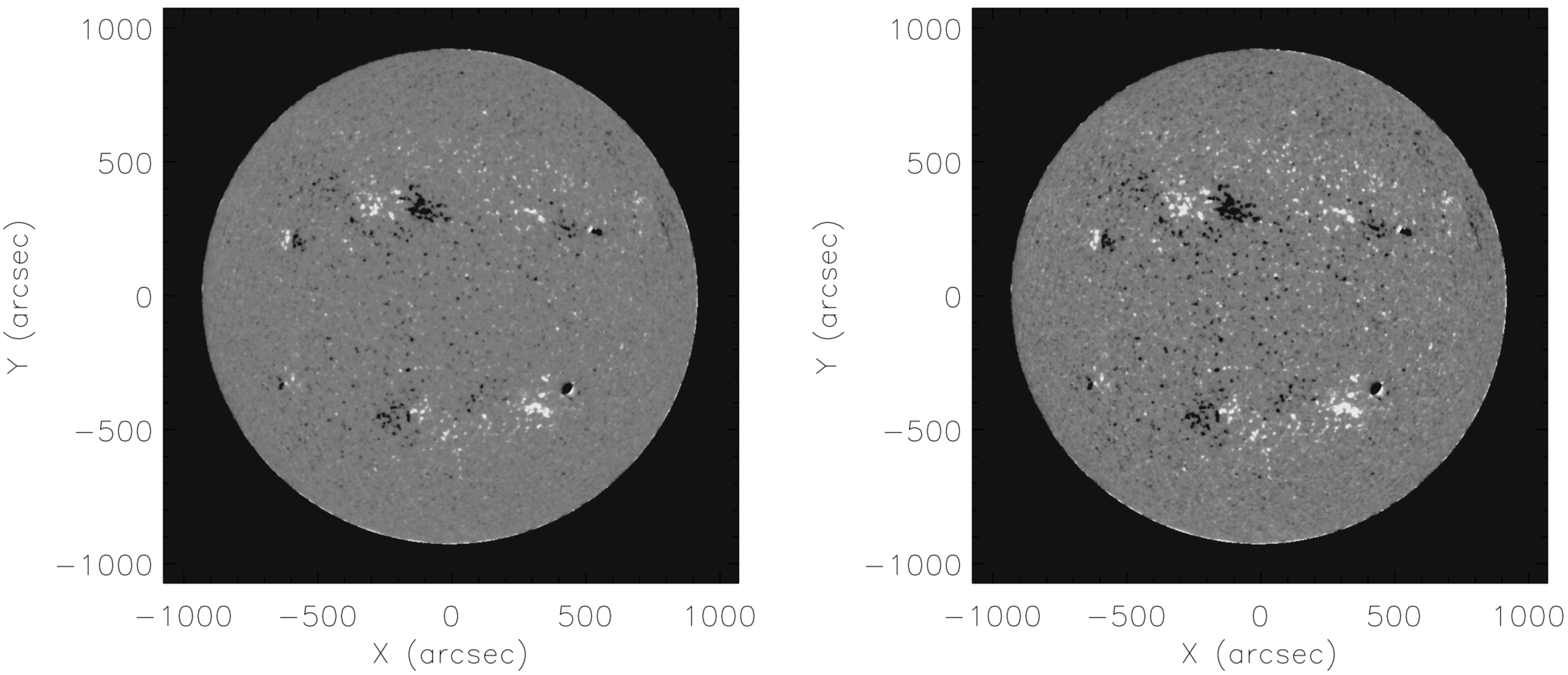

GONG magnetogram from 4 July 2009 (left) and calibrated magnetogram (right), saturated at ±50G.

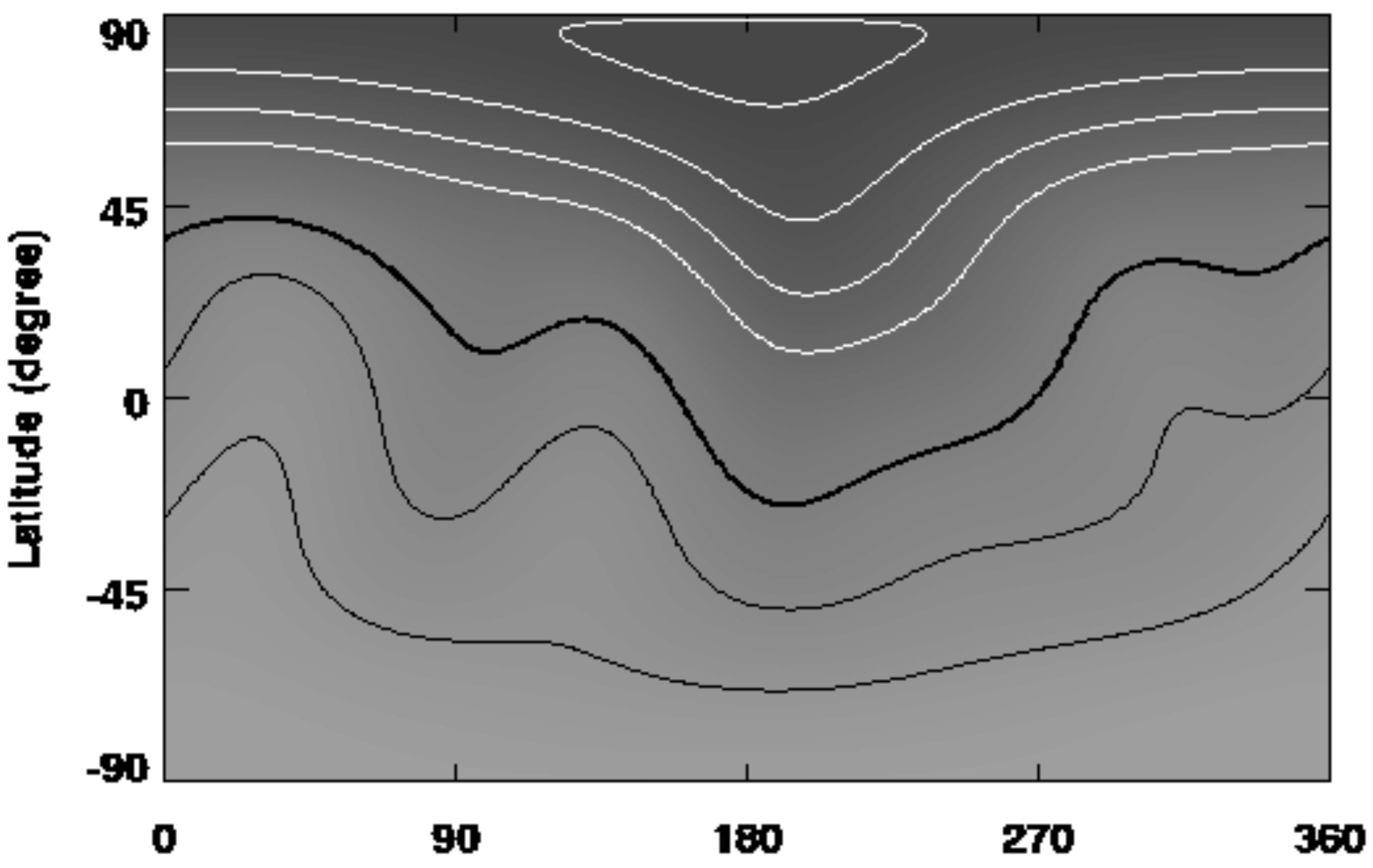

Carrington Rotation 2098 (July 2010):

Contour plots of PFSS flux distribution at outer boundary (2.5 solar radii). Contours are 0.02 G apart.

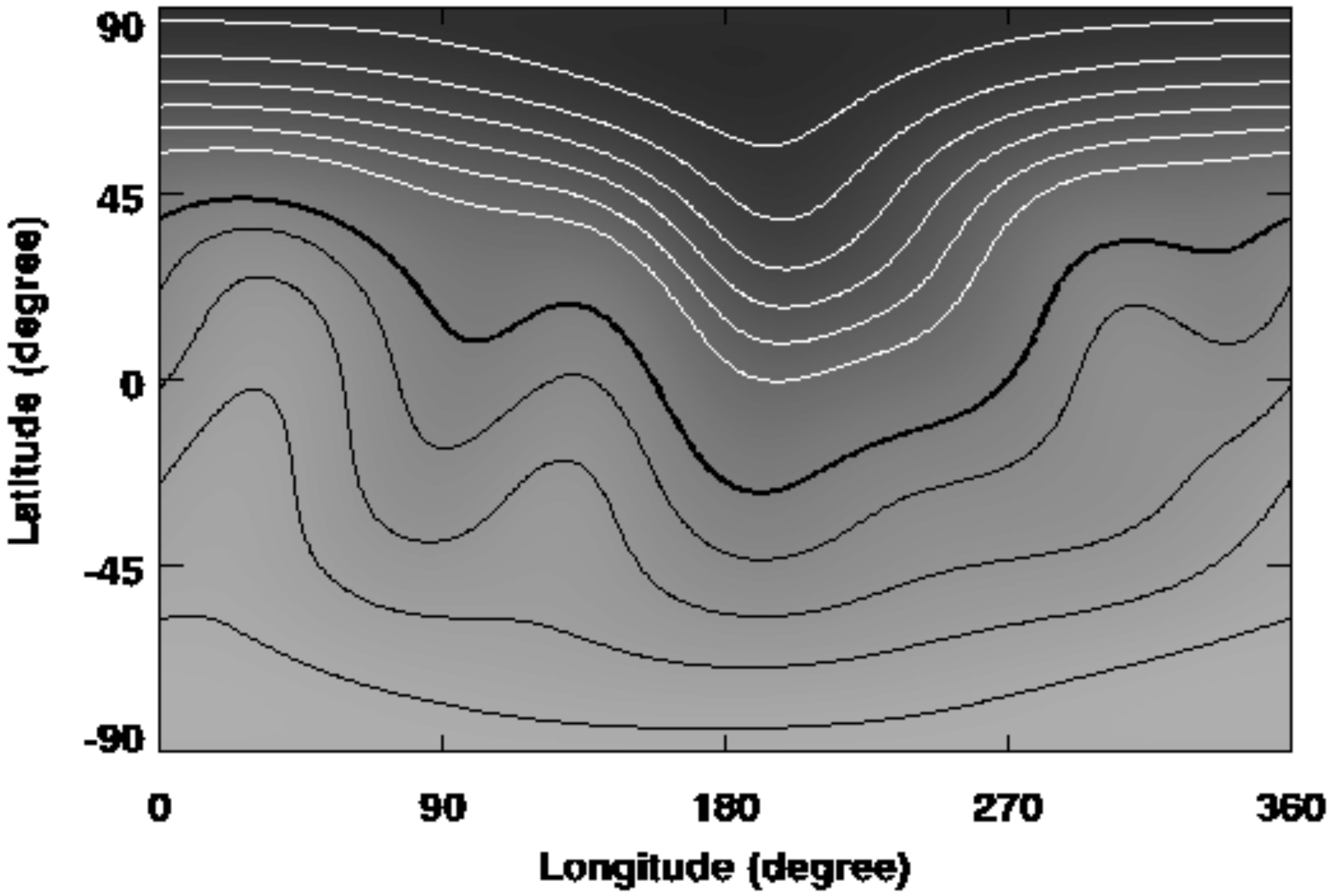

The open flux for the initial data (top) is 1.17 x 10^{22} Mx.

The PFSS open flux for the calibrated magnetograms (bottom) is 1.76 x 10^{22} Mx.

Summary

- The standard ingredients of the Babcock-Leighton model for the cycle (asymmetric tilted bipolar active regions, polarity-biased poleward surges, polar fields' response) remain evident.
- Cycle 24 has had weaker and more asymmetric activity than the previous three cycles, including cycle 23.
- Cycle 24 polar fields are of similar strength as cycle 23 poles, about 60% as strong as cycle 21, 22 polar fields.
- High-resolution Hinode SOT/SP vector field observations show that stronger kG structures define the dominant polarity of the pole and its reversal. Suspicion of undetected flux at highest latitudes where effective spatial resolution is lower - requires further study.
- Combining data from different telescopes is increasingly necessary, but risky. A solar gauss is an unknown quantity. Pursuing solution using end-to-end simulation of GONG magnetogram observation.